Electrochemical Energy Reviews (2020) 3:187–219
https://doi.org/10.1007/s41918-019-00058-y

REVIEW ARTICLE

Advanced Characterizations of Solid Electrolyte Interphases in Lithium-Ion Batteries

Yanli Chu[1,2] · **Yanbin Shen**[2] · **Feng Guo**[1,2] · **Xuan Zhao**[2] · **Qingyu Dong**[2] · **Qingyong Zhang**[3] · **Wei Li**[3] · **Hui Chen**[3] · **Zhaojun Luo**[3] · **Liwei Chen**[2,4]

Received: 15 February 2019 / Revised: 21 April 2019 / Accepted: 24 October 2019 / Published online: 21 November 2019
© Shanghai University and Periodicals Agency of Shanghai University 2019

Abstract

Solid electrolyte interphases (SEIs) in lithium-ion batteries (LIBs) are ionically conducting but electronically insulating layers on electrode/electrolyte interfaces that form through the decomposition of electrolytes. And although SEIs can protect electrodes from the co-intercalation of solvent molecules and prevent the continued decomposition of electrolytes, their formation can consume active lithium and electrolytes and build up impedance for ion conduction. Therefore, the control of SEI structures and properties to allow for stability and ionic conductivity has become a critical but highly challenging task in battery designs. However, several factors contribute to the difficulty in SEI research. First, the chemical and electrochemical reactions leading to SEI formation are immensely complex and heavily influenced by numerous factors including electrolyte solvents, lithium salts, additives, electrode materials and charge/discharge conditions. Second, the chemical nature of film-formation products such as SEI constituents and their distribution and arrangement in the SEI are complex. Finally, SEIs are in situ formed at the electrode/electrolyte interface in assembled batteries, making the direct observation of SEIs difficult. To address these challenges, the development of advanced characterization techniques is key in the fundamental understanding of SEIs in LIBs. Based on this, this review will provide an overview of the progress in SEI characterization, including methods to investigate electrochemical performance, surface morphology, chemical composition, and structure and mechanical properties, with state-of-the-art characterization techniques developed in recent years being emphasized. And overall, the scientific insights obtained by using these advanced methods will help researchers to better understand electrode/electrolyte interfaces toward the development of high-performance secondary batteries.

Keywords Lithium-ion batteries · Solid electrolyte interphase characterization · Mechanical elasticity · AFM force curve · ToF–SIMS · Cryo-TEM · IR-aNSOM

1 Introduction

Since being introduced by Sony in 1991, lithium-ion batteries (LIBs) employing carbon-based anodes and transition metal oxide cathodes have become widely adopted due to high energy densities and good cyclability [1]. Currently, LIBs are the most widely used electrochemical energy storage devices for portable electronics and power tools. However, ever-growing energy storage demands driven by rapid developments in electric vehicles and renewable electricity sources in recent years have generated increasing interest in the exploration of energy storage systems with higher capacities, better safety and lower costs [2–5].

During the development of the original LIB, the resolution of problems associated with the electrode/electrolyte interface on anodes was a vital step. Back in the 1970s

✉ Yanbin Shen
ybshen2017@sinano.ac.cn

✉ Liwei Chen
lwchen2008@sinano.ac.cn

[1] School of Nano Technology and Nano Bionics, University of Science and Technology of China, Hefei 230026, Anhui, China

[2] i-Lab, CAS Center for Excellence in Nanoscience, Suzhou Institute of Nano-Tech and Nano-Bionics (SINANO), Chinese Academy of Sciences, Suzhou 215123, Jiangsu, China

[3] Shenzhen Bak Battery Co., Ltd, Shenzhen 518119, Guangdong, China

[4] In-situ Center for Physical Sciences, School of Chemistry and Chemical Engineering, Shanghai Jiao Tong University, Shanghai 200240, China

when lithium metal was the most popular anode material for lithium batteries, Dey et al. [6] reported the existence of a passivation layer on lithium metals soaked in nonaqueous electrolytes. Subsequently, Peled et al. [7] discovered in 1979 that this passivation layer was ionically conducting but electronically insulating and named this layer as the solid electrolyte interphase (SEI). And aside from dendritic problems caused by uneven lithium deposition, lithium metal was found to suffer from unstable SEIs due to the large volume change of lithium metal during cycling, in which the repair of the SEI consumed active lithium and electrolytes, leading to rapid capacity fading, which remains a major obstacle for the application of lithium metal anodes even today. In the 1990s however, Sony found that graphite, a cheap and stable material in nonaqueous electrolytes, could be used as an intercalation host for Li^+ similar to $LiCoO_2$ cathodes and possessed a low intercalation potential for Li^+ that was close to the lithium reduction potential. This led to the immediate use of graphite as an anode material to replace lithium metal and thus emerged the so-called rocking chair LIB, in which Li ions are shuttled back and forth between a $LiCoO_2$ cathode and a graphite anode in a carbonate-based electrolyte (i.e., $LiPF_6$/propylene carbonate (PC)). Despite this, researchers soon found that without a passivation layer on the graphite anode, carbonate molecules were transported with Li^+ as a solvation shell and co-intercalated into graphite, which damaged anode structures and resulted in short-cycle life spans. This problem was subsequently solved by replacing PC-based solvents with ethylene carbonate (EC)-based solvents that can be reduced at a certain potential to form a passivating SEI layer that can de-solvate Li^+ and prevent the exfoliation of graphite, ultimately leading to the commercialization of LIBs [8, 9]. And based on this, it can be seen that the SEI is a critical component of current LIBs.

Because the formation of the SEI layer consumes active Li^+ and electrolytes and can also increase the resistance of Li ion diffusion into graphite, the formation of the SEI with a stable structure and good ionic conductivity is essential in optimal battery designs. Because of this, researchers are constantly seeking new methods to regulate the SEI structure to achieve less irreversible capacity loss and reduce interfacial resistances to enhance battery performance. And with tremendous efforts in the investigation of SEIs since the 1970s, it is now well recognized in both academic and industrial communities that the properties of SEIs can affect cycle life, power capability and even safety in LIBs [10–16]. Despite this, the in-depth understanding of SEIs with enough detail information remains lacking (i.e., chemical compositional structure from the molecular level to the nanoscale building block level). This is because the characterization of SEIs is extremely challenging due to several factors. One factor is that SEI formation reactions, which occur along with Li intercalation and are affected by numerous factors including electrolyte composition and charge/discharge conditions, meaning that SEI chemical compositions and structures are complex. In addition, thin SEI layers are buried between two electrodes inside a battery and become unstable and "dead" after being taken out from the volatile electrolyte in the LIB. Furthermore, there are insufficient direct measurements of SEI physical properties. Therefore, the characterization and understanding of SEIs and the correlation between SEI physical properties and battery performances are critically important but remain immensely challenging. And without fundamental understanding, most efforts on the regulation of SEIs can only be conducted through trial-and-error processes. However, LIB manufacturers have already accumulated substantial knowledge on SEI formation, leading to standard production protocols to form stable SEIs, including charging the battery at low current densities after battery assembly, which can be referred to as "formation" [17–19], and adding electrolyte additives that are more easily reduced or oxidized than electrolyte solvents to form a SEI/CEI with designed components [20–27]. And with the help of these approaches, the formation of SEIs in current commercial LIBs is relatively "controllable". However, irreversible capacity loss due to SEI formation and repair remains one of the main causes for capacity decay in current LIBs. And in particular for high-energy density LIBs using nickel-rich layered oxides as the cathode and Si as the anode, the electrolyte can become severely oxidized on cathode surfaces to form a cathode electrolyte interphase (CEI) and the SEI layer on the anode is also not stable during cycling due to the large volume expansion of Si. Furthermore, the development of next-generation battery systems using lithium metal anodes (e.g., Li–S, Li–O_2 batteries) also requires the fundamental understanding of SEIs on lithium anodes. Therefore, techniques to obtain fundamental understandings of SEIs are urgently needed to optimize the design of SEIs and enhance the performance of LIBs, especially for the development of next-generation lithium batteries.

To optimize cycle life and power density in batteries, the perfect SEI should be thin (to minimize the consumption of active lithium and the resistance for Li ion conduction), dense (for the insulation of electrons), possess uniform morphology and structure (for uniform Li ion conduction), be (electro)chemically stable (to prevent the need for repairs) and mechanically flexible (to buffer volume expansion of active materials) [28]. And to design these optimal SEIs, characterizations based on morphology, mechanical elasticity, chemical composition and structure, especially with molecular- to nanometer-scale spatial resolution, as well as the in operando investigation of the evolution of these physical properties during growth and cycling are vital in which SEI research in the past few decades has accumulated considerable mastery on the ex situ and in situ characterization of morphology, chemical composition, structure and formation.

In the characterization of SEIs, traditional characterization techniques such as electrochemical impedance spectroscopy (EIS), differential capacity (d*Q*/d*V*), linear sweep voltammetry (LSV) and cyclic voltammetry (CV) have been commonly used to investigate the formation and impedance [29–33], whereas scanning electron microscopy (SEM), transmission electron microscopy (TEM) and atomic force microscopy (AFM) have been intensively used to observe surface features and morphology in the meso- to nanoscale [34–40]. In addition, X-ray photoelectron spectroscopy (XPS), Fourier transform infrared spectroscopy (FTIR) and secondary ion mass spectrometry (SIMS) are often used to study chemical composition and structure [41–45]. In recent years however, novel characterization techniques have also been adopted to investigate SEIs at high spatial resolution close to the chemical building block and in states that are close to "alive" SEIs. For example, AFM force curves have been used to measure the mechanical elasticity and structure of SEIs with nanometer resolution [46–49], and apertureless near-field scanning optical microscopy (aNSOM), which employs an AFM tip that is in contact with the measured material surface as an optical probe for high-resolution spectroscopy and imaging measurements, has also been applied to map the chemical composition of SEIs [50, 51]. In addition, time-of-flight secondary ion mass spectrometry (ToF–SIMS) was found to be useful in the construction of depth profiles for chemical components [52–54]. And since 2017, cryo-scanning transmission electron microscopy (cryo-STEM), originally designed to preserve hydrated biological specimens, has been introduced to investigate the chemical composition and structure of SEIs and has produced exciting results [55–59].

And based on all these developments, this review will summarize the common knowledge distilled from SEI research in the last few decades and discuss examples reported in the literature concerning the use of traditional characterization techniques to investigate SEIs, including electrochemical performance, morphology and chemistry. This review will also present state-of-the-art SEI characterizations by using advanced techniques such as in situ ToF–SIMS, IR-aNSOM, cryo-TEM and AFM force curves. Overall, the goal of this review is to promote the future characterization of interfaces in batteries and to advance the electrochemistry of high-density, high-performance energy storage systems.

2 Overview of SEIs in LIBs

2.1 Formation

Electrolyte components will reduce on anode surfaces if their lowest unoccupied molecular orbital (LUMO) is lower than the Fermi level of the anode, leading to the deposition of insoluble reduction products on the anode surface to form an SEI layer (Fig. 1a) [60]. Similarly, electrolyte components will oxidize if their highest occupied molecular orbital (HOMO) is higher than the cathode Fermi energy level to form a CEI layer. This reduction and oxidation will continue until electron leakage is stopped by a passivating SEI/CEI layer. And due to the complex environments of

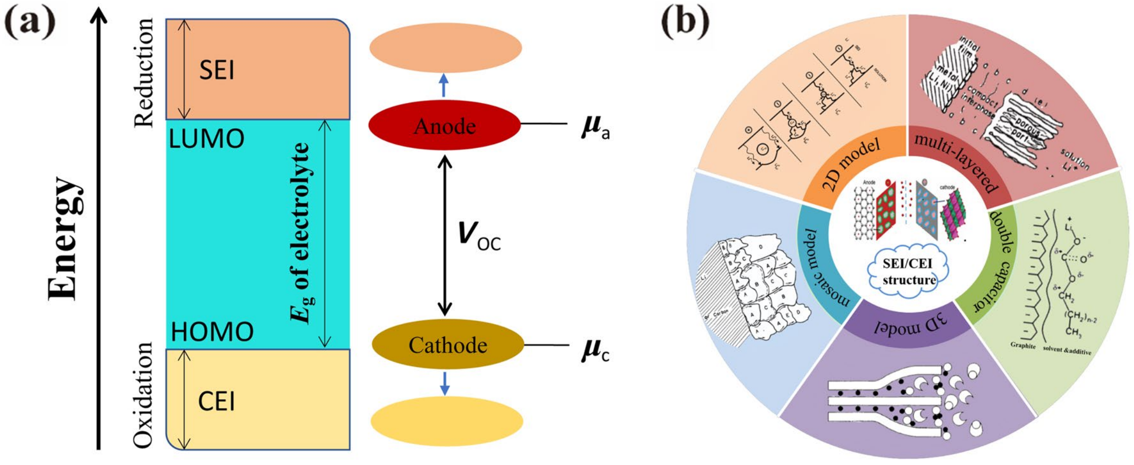

Fig. 1 **a** Schematic of the SEI and CEI formation mechanism. Reproduced with permission from Ref. [60]. Copyright 2009, American Chemical Society. **b** Models of SEI structures: the 2D model is reproduced with permission from Ref. [7]. Copyright 1979, The Electrochemical Society; the mosaic model is reproduced with permission from Ref. [62]. Copyright 1997, The Electrochemical Society; the 3D model is reproduced with permission from Ref. [8]. Copyright 1995, Elsevier; the double-capacitor model is reproduced with permission from Ref. [63]. Copyright 1999, The Electrochemical Society; the multilayered model is reproduced with permission from Ref. [64]. Copyright 1995, Elsevier

the electrolyte, which contains salts, solvents and various additives, the reduction and oxidation potentials of electrolyte components shift significantly from calculation values or electrochemical standard values. (Computed reduction potentials for several common solvents, additives and solvated ions have been summarized by Delp et al. [61].) And in practice, reduction and oxidation potentials are also considerably affected by charge/discharge conditions and surface properties of electrode materials.

2.2 Structure

SEI layers possess complex and heterogeneous substructures, and in the last few decades, researchers have proposed several structural models for SEIs (Fig. 1b) in which a "2D model'" was the earliest proposed for an SEI on the surface of a lithium metal anode [7] followed by a "3D SEI" model proposed for an SEI on the surface of a graphite anode [8]. Subsequently, Peled et al. [62] conducted chemical analysis of SEIs and modified the previous "2D model" to propose a "mosaic model" in which salts were found to be deposited in separate lumps. Ein-Eli et al. [63] also proposed a "double-layer capacitor model" for SEI structures in which solvents and additives produced an efficient passivation film and fixed positive charges in SEIs to counter negatively charged graphite. And with the help of EIS and FTIR spectroscopy, Zaban et al. [64] proposed a "multilayered model" for SEI structures in which the SEI morphology possessed a thickness of 15–100 Å, a compact inorganic inner layer (i.e., LiF, Li_2O, Li_2CO_3) and a porous organic outer layer (i.e., ROLi, $ROCO_2Li$). Here, the researchers suggested that the conductivity of the porous organic outer layer was lower than that of the compact inorganic inner layer, and as a result, as the organic outer layer grows thicker, the electrolyte molecules stop receiving electrons from the electrode for further reduction, resulting in the self-termination of SEI growth. Currently, this model has gained wide acceptance among the scientific community and has been verified by several experimental and theoretical investigations [52, 65–68]. As for lithium diffusion in this "multilayered model" for SEIs, two different mechanisms have also been proposed for the outer and inner layers [52, 69–71] in which Li^+ can rapidly pass through the porous organic region together with anions that have been dissolved in the electrolyte in order to maintain local electric neutrality and follow Fick's law. Alternatively, only Li^+ can move across the compact inorganic layer through vacancies or interstitial sites through direct hopping and repetitive "knockoff" of Li^+ on lattice sites. Researchers have also reported that below 0.98 V, the main diffusion carriers in the dense layer were Li^+ interstitials, whereas above 3.98 V, Li^+ vacancies made greater contributions. And in the range of 0.98–3.98 V, Li^+ vacancies and Li^+ interstitials both played important roles. Researchers have also reported that the main diffusion carriers in the compact layer of SEIs were Li^+ interstitials, whereas those in CEIs were Li^+ vacancies [71]. Moreover, researcher have also demonstrated that battery performances can be enhanced with multilayered SEIs, which can be achieved through the polishing of lithium electrodes [72] and the addition of electrolyte additives [59]. Furthermore, researchers have reported that the thicknesses of freshly formed SEIs are usually in the ranges of 30–100 Å and 5–10 Å for CEIs [42]. This difference in thickness is possibly due to the extent of secondary reactions and the electrochemical stability window of electrolyte solvents and salts in which currently used electrolytes are more prone to solvent reduction on anodes rather than oxidation on cathodes [73].

2.3 Chemical Composition

The chemical composition of SEIs/CEIs is largely dependent on factors such as the surface property of electrode materials, the electrolyte composition and the impurities in the battery, especially H_2O, which can be introduced from the environment during cell assembly. And among these factors, electrolyte composition is the most direct factor deciding SEI/CEI chemistries. Here, LIB electrolytes usually consist of one or more conducting lithium salts (e.g., $LiClO_4$, $LiPF_6$, $LiBF_4$, $LiAsF_6$) dissolved in single or mixed nonaqueous solvents including cyclic and acyclic carbonates such as EC, PC, diethyl carbonate (DEC) and ethyl methyl carbonate (EMC). In addition, numerous additives are also present in electrolytes such as vinylethylene carbonate (VEC), vinylene carbonate (VC) and fluoroethylene carbonate (FEC). And overall, it is generally accepted that the chemical composition of SEIs contains both inorganic and organic compounds. In electrolytes composed of lithium salts dissolved in carbonate solvents, the inorganic constituents of SEIs usually include Li_2O, LiF and Li_2CO_3, whereas the organic constituents include $ROCO_2Li$ and ROLi ($R = CH_3$–, CH_3–CH_2–, CH_3–CH_2–CH_2–, etc.) [74–77]. Here, the inorganic constituents of SEIs vary greatly based on the different types of salts used in the electrolyte [78–80]. For example, in electrolytes containing LiTFSI salt, –SO_2-containing species or possibly $LiSO_4$ usually appears in the SEI film. And if $LiPF_6$ salt is used, Li_xPF_y and $Li_xPO_yF_z$ are found in the inorganic layer of the SEI. Moreover, inorganic constituents generally exist in the inner layer of SEIs, whereas organic constituents are mostly found in the outer layer [52, 81, 82]. And on the anode side, the chemical composition of SEIs remains similar regardless of the reaction mechanisms involved in the charge storage process in which only in the case of Si-based alloying anodes can the presence of siloxanes and SiO_xF_y in the SEI be detected, whereas other organic and inorganic components remained the same as in other anodes [83]. Similarly, the chemical compositions of cathode CEIs and anode

SEIs are almost the same except that lithium oxides and lithium alkoxides are only found in anode SEIs and transition metal oxides and organometallic components are mostly found in CEIs due to the removal of oxygen from cathode material lattices and reactions on the interfaces [42, 84, 85].

2.4 Factors Affecting SEI Properties

The composition of SEIs is directly related to electrolyte composition in which in carbonate electrolytes, the most observed SEI component is a mixture of Li_2CO_3 and semi-carbonates (also called alkylcarbonate), whereas in ether electrolytes, the most observed SEI component is lithium alkoxides [86–89]. Here, semi-carbonates are a result of the single-electron reduction of carbonate solvents and can be further reduced into oxalates by lithiated graphite, which can be significantly promoted at elevated temperatures [90, 91]. In addition, the decomposition products of various solvents depend on the properties of the solvent itself, such as reactivity, viscosity, the dielectric constant, polarity and so on. The reactivity of common carbonate-based electrolytes is in the order of $EC > PC > DMC > DEC$ [92]. Furthermore, the concentration and preferential reduction of mixture carbonates can also affect the constituents of SEIs [93, 94]. Film-forming additives can also significantly alter reaction pathways and SEI properties [95] in which aside from commonly used film-forming additives such as VC, VEC and FEC, other inorganic and organic substances such as polysulfides S_x^{2-} [96], LiI [97], Li_2CO_3 [98], acrylic acid nitrile (AAN) [99] and 1,3-propane sultone (PS) [100] can also be used. For example, Aurbach et al. [92, 101, 102] reported that the enhanced Li_2CO_3 content in SEIs and improved battery performances can be obtained through the use of CO_2 as an additive. Impurities can also affect SEI formation in which trace amounts of water present in electrolytes can affect SEI composition if water-sensitive salts are used. Here, for electrolytes containing LiTFSI salts, which possess much better thermal and chemical stability than $LiPF_6$, the presence of water does not affect SEI components [103, 104]. However, for $LiPF_6$-based electrolytes, trace amounts of water can react with $LiPF_6$ and generate HF, which can decompose major components in SEIs and consume Li^+, leading to capacity decay. In addition, generated HF can corrode electrode materials and current collectors [105–108].

Different electrode materials have different effects on the chemistry and structure of SEIs. For example, although SEIs formed on graphite anodes may be stable, similar electrolytes and formation conditions may generate SEIs that are unstable on Si anodes due to large volume changes in cycling [109, 110]. And aside from chemical nature, other factors in anode materials such as specific surface area, crystallographic structure, particle morphology, defect concentration and nature and exposed crystalline planes can also affect SEIs [111–115] in which SEIs on the edge plane of graphite particles generally contain more inorganic components such as LiF, whereas SEIs on the basal plane contain more soft organic compounds [79, 116–118]. Therefore, the edge-to-basal-plane ratio of anode materials is also a factor affecting SEI properties.

The electrochemical conditions in the initial cycle of LIBs also play a critical role in SEI formation. These conditions include factors such as charge/discharge current density, polarization, temperature and shelving time [93, 119–121]. In addition, two types of reactions can occur at elevated temperatures in which one is the transformation of the SEI, which involves components such as lithium alkyl carbonates and semi-carbonates being turned into stabler components such as Li_2CO_3. As for the other reaction, this involves multiple reactions between active materials and SEIs, SEIs and electrolytes or electrolytes and active materials [122, 123], most of which are exothermic and detrimental to the performance of LIBs, especially in terms of safety. Furthermore, influences from contamination, air and humidity on SEI chemistry are also significant, for example, $ROCO_2Li$ and ROLi can convert to Li_2CO_3 through reactions with CO_2, and $ROCO_2Li$ can react with water to form Li_2CO_3, CO_2 and ROH. In addition, other alkyl lithium carbonates can also react with water to form LiOH or Li_2CO_3 [124, 125].

3 Advanced Characterizations of SEIs

3.1 Electrochemical Characterization

Electrochemical characterization techniques such as EIS, dQ/dV, LSV, CV and electrochemical quartz crystal microbalance (EQCM) are essential for the direct investigation of electrochemical performances for SEIs during formation and evolution. In the case of EIS, it can provide important insights into electrolyte resistance, ionic diffusion impedance, electrode kinetic and double-layer capacitance in complex electrochemical systems such as LIBs in which a reasonable equivalent circuit model is usually needed to diagnose EIS spectra properly. Here, typical equivalent circuit models proposed for secondary batteries include an R_e (the bulk resistance of the cell that reflects the combined resistances of the electrodes, the electrolyte and the separator), an R_{sei} and a C_{sei} (the resistance and capacitance of the SEI/CEI corresponding to the semicircle in the high frequency range), an R_{ct} and a C_{dl} (the charge transfer resistance and its relative double-layer capacitance corresponding to the semicircle in the medium frequency range) and a W (the Warburg impedance that is related to the diffusion of Li^+ in the material bulk) and are also dependent on the battery system [32, 126]. For example, based on the knowledge that the formation and growth of SEIs are accompanied by changes in R_{sei}, Zhang et al. [32] used EIS as an in situ tool to investigate SEI formation in Li||graphite cells in which they investigated the correlation between R_{sei} and cell voltage and found that R_{sei} varied significantly with cell voltage. Here, the researchers reported that the R_{sei} of the SEI increased significantly with lithiation and decreased reversibly in subsequent de-lithiation between 0.15 and 0.04 V and proposed that the formation of the SEI can be divided into two voltage regions based on the evolution of R_{sei} during the initial lithiation in which the SEI formed above 0.15 V was less conductive and the SEI formed below 0.15 V was highly conductive. In addition, these researchers also observed the effects of electrolyte chemistry on the R_{sei} of the Li||graphite cell and reported that the ionic conductivity of the preliminarily formed SEI was largely dependent on the types of solvents and salts of the electrolyte in which the R_{sei} decreased in the order of $LiBF_4 > LiSO_3CF_3 >$ lithium bis(oxalato) borate (LiBOB) $> LiPF_6$ for salts and NMP > EMC > MB for solvents. Moreover, these researchers also reported that the addition of VC into the electrolyte resulted in a considerable increase in the R_{sei}.

To obtain more precise results, Friedrich et al. [127] used the distribution of relaxation time (DRT) from measured spectra as an auxiliary means of EIS analysis to study SEI formation at different SOCs and temperatures and reported that the comparison of R_{sei} during the first and the second lithiation cycles showed maximum SEI resistance in the voltage region between 0.8 and 0.3 V versus Li/Li^+ during the first lithiation process that was not present during the second lithiation, indicating that the formation of an SEI with high Li^+ conductivity is completed after the first cycle. In addition, temperature-dependent measurements in this study showed that the overall resistance decreased with increasing temperatures between 20 °C and 45 °C, which the researchers attributed to the temperature-dependent charge transfer and ion transport in the electrolyte and SEI. However, these researchers also reported that at 55 °C, the overall resistance increased as compared with that at 45 °C, indicating undesirable thermally induced resistances. In another study, Heins et al. [29] calculated the activation energy of electrochemical processes based on temperature-dependent impedance spectra and found that during the first charging cycle, the structural and chemical compositions of SEI films on graphite surfaces can change with the increasing SOC in which SEI films with low SOC possessed higher impedance and lower activation energy, whereas SEI films with high SOC possessed higher ionic conductivity and higher activation energy. These researchers also reported that after obtaining a stable SEI film, the activation energy change of the SEI film was small under different charged states.

Aurbach et al. [33] also used EIS to investigate the SEI on graphite electrodes cycled in a 1.0 M $LiAsF_6$/EC + DMC (1:1) electrolyte with VC additives and reported that the addition of VC can reduce R_{sei} and overall resistances at 25 °C. However, these researchers also reported that at 60 °C, the R_{sei} and overall resistance of the SEI formed in the presence of VC were higher than those formed in VC-free electrolytes. Here, the researchers attributed the higher resistances to the formation of poly-alkyl Li-carbonate species that can suppress the reduction of both solvents and anions. Furthermore, Xu et al. [21] found that FEC additives can reduce the room-temperature overall impedance of SEIs on silicon anodes cycled in 1.0 M $LiPF_6$/EC + DEC (1:1) electrolytes.

EIS can also be applied to investigate CEIs on cathodes. For example, Zhang et al. [128] studied the property and evolution of CEIs formed in $LiCoO_2$||Li cells and reported that the semicircle at the high-frequency region of the obtained EIS spectra showed little change, whereas the semicircle at the intermediate-frequency region enlarged sharply as the cell cycled, indicating that the CEI layer was stabilized after several cycles but that the aging of the electrode resulted in further increases in cell resistance. In addition, Sun et al. [129] applied EIS to investigate the synergistic effects of FEC and hexamethylene diisocyanate (HDI) on CEI formation on a $LiNi_{0.5}Mn_{1.5}O$ cathode and found that CEI impedances decreased significantly with the addition of 25 mM HDI as compared with that of the baseline electrolyte, but increased with the addition of 500 mM HDI. Zhao et al. [130] also studied the effects of additives on a $LiNi_{0.76}Mn_{0.14}Co_{0.10}O_2$ (NMC76) cathode using EIS in which by comparing the EIS spectra of cells with the baseline electrolyte (1 M $LiPF_6$/EC–EMC) and an optimized electrolyte [0.6 M LiTFSI + 0.4 M LiBOB + 0.05 M $LiPF_6$ dissolved in EC:EMC (4:6, in weight ratios)] during 200 cycles, it was found that surface film resistances remained small throughout cycling but charge transfer impedances increased with cycles in the baseline electrolyte, whereas surface film resistances were initially large but subsequently decreased in the optimized electrolyte, with charge transfer impedances only slightly increasing during cycling. Here, the researchers attributed the difference in the two electrolytes to the fact that the CEI film formed in the optimized electrolyte was more conductive, more compact and stabler as compared with the base electrolyte.

LSV and CV are complementary electrochemical methods and together, can provide more details concerning the reactions of electrolytes with electrode surfaces. As a result, LSV and CV have been used to understand SEIs. For example, Yoon, et al. [30] used LSV in a three-electrode cell (the Pt disk, Li foil and Pt wire were used as the working, the reference and the counter electrodes, respectively) to examine N-substituted caprolactam (CL) derivatives as SEI-forming additives and found that the reduction potentials derived from dQ/dV curves for acetyl-CL, ξ-CL, methyl-CL, vinyl-CL and VC were 1.02, 0.78, 0.82, 1.10

and 1.05 V, respectively. In another study, He et al. [131] used CV to study the activation characteristics and current density effects on SEI formation in Li||graphite, Li||$LiCoO_2$ and graphite||$LiCoO_2$ cells and Zheng et al. [132] used CV to investigate the effects of typical impurities (different volumetric concentrations of water and CH_3OH) in an electrolyte system of 1.0 M $LiPF_6$/(EC + DMC + EMC) on the formation of SEI films on the surface of MCF (mesophase-pitch-based carbon fiber) negative electrodes. Furthermore, Zhang et al. [133] used CV to determine the reduction potentials of EC, PC, DEC, DMC and VC using inert electrodes in a $LiClO_4$/tetrahydrofuran (THF) electrolyte and reported that each solvent possessed its own reductive peak related to its reaction pathway and that the experimental potentials of EC, DEC, PC, DMC and VC were 1.36, 1.32, 1.0–1.6, 1.32 and 1.4 V, respectively. Moreover, Ota et al. [24] compared the CV curves of graphite electrodes recorded in 1.0 M $LiPF_6$/EC + DMC (1:1), 1.0 M $LiPF_6$/EC + DMC (1:1) +2 wt% VC and 1.0 M $LiPF_6$/VC and found that the cathodic peaks of EC and VC appeared at 0.7 and 1.1 V versus Li/Li^+ and that $(CHOCO_2Li)_2$, $(CH{=}CHOCO_2Li)_2$, $(CH{=}CHOLi)_2$ and RCOOLi were formed on graphite as VC reduction products. These researchers also found that the presence of VC in the EC-based electrolyte can decrease the evolution of reductive gases such as C_2H_4, CH_4 and CO. Aurbach et al. [33] also found that VC can suppress irreversible charge in the first cathodic process at both 25 and 60 °C, which can enhance cycle life. Moreover, Kjell et al. [134] used LSV and CV to study SEI growth on silicon anodes in a 1.0 M $LiPF_6$/EC + DEC(1:1) electrolyte and found that SEI formation started at 1.4 V and continued to form on the electrode in the following second–fourth cycles, which was different from SEI formation on graphite electrodes. In addition, Lindgren et al. [135] found that the reductive decomposition of FEC on silicon electrodes occurred at ~ 1.3 V (vs. Li/Li^+) and that FEC can form a stable SEI before EC and DEC to avoid large cracks on the electrode and suppress continuous SEI formation.

Overall, the techniques mentioned above are widely used in the research of batteries; however, it is difficult to quantify chemical components during SEI formation. To address this, electrochemical quartz crystal microbalance (EQCM), which can detect sensitive changes in electrode masses as small as a few nanograms, has been adopted to study SEI formation. For example, Aurbach et al. [33] used EQCM and CV to study SEI formation on graphite electrodes in a 1.0 M $LiAsF_6$/EC + DMC (1:1) electrolyte. Here, the researchers reported that both voltammograms showed that the onset potential of the reduction process was below 2.5 V (vs. Li/Li^+) and that as compared with VC-free electrolytes, mass accumulation on the electrode in an electrolyte with VC additives was 50% higher. Liu et al. [31] also studied SEI formation on graphite electrodes in a carbonate electrolyte using EQCM and proposed that the cathodic polarization of graphite can be divided into four regions based on the mass change results recorded by EQCM during SEI formation. These four regions include region I (above 2.4 V) in which both current and mass changes remained essentially at the background baseline; region II (2.4–1.1 V) in which the current started to depart from the background and reached a local maximum at ~ 1.6 V accompanied by mass change, which could be the onset of certain reactions; region III (1.1–0.74 V) in which a broad current response occurred, which could correspond to the initial decomposition of electrolyte components; and region IV (0.74–0.0 V) in which the major electrochemical reduction of intercalated species, the exclusive decomposition of the liquid electrolyte and the formation of the eventual SEI occur.

3.2 Morphological Characterizations

Ideally, SEI/CEI layers should be thin and dense and can uniformly cover electrode surfaces and remain stable during cycling, so as to effectively and evenly conduct Li^+ but insulate electrons to prevent the electrolyte from further decomposition. Here, SEM, TEM and AFM are common techniques used for the imaging of the morphology of interphases in which both SEM and TEM require high vacuums to operate and therefore are not usually suitable for the in situ study of SEIs/CEIs in electrolytes. Alternatively, AFM is a scanning probe microscopy technique that is capable of studying liquid–solid interfacial morphology with nanometer-scale spatial resolution.

3.2.1 Morphological Characterization by SEM

SEM is a common microscopic characterization technique in materials science, and in addition to morphological imaging, SEM-based energy spectroscopy techniques such as energy-dispersive X-ray analysis (EDX) can provide quantitative information about local elemental compositions. Based on this, numerous studies have been conducted on the dependence of SEI morphology on electrolytes, electrode materials and electrochemical cycling conditions by using in situ and ex situ SEM [34, 35, 41, 135–142] in which as early as 1996, Kominato et al. [140] found by using SEM the morphology of surface films formed on lithium metal deposited on a nickel substrate in an EC/DMC-based electrolyte is dependent on electrolyte salts ($LiPF_6$, $LiClO_4$ and LiTFSI). In addition, Lee et al. [34] applied extremely high-resolution SEM using low acceleration voltage to avoid electron beam-induced damage to visualize SEI layers on a graphite anode and obtained the outermost surface and cross-sectional SEM images of the graphite anode before and after low-energy ion etching. As a result, these researchers found that the fine particles were present in a dense surface film and that after 5 min of etching, the SEI layer was almost completely removed except for the particles, which was attributed to the difference between the film thickness and the particles (Fig. 2a).

Although SEM measurements require high-vacuum environments and are therefore usually unsuitable for in situ observations of SEIs, in situ SEM can be achieved by using special sample transfer chambers and ionic-liquid (IL) electrolytes. For example, Strelcov et al. [35] investigated the formation of the SEI on the surface of a V_2O_5 nanowire anode during the in situ SEM study of lithium intercalation in a V_2O_5-based single-nanobelt battery with a $LiCoO_2$ cathode and an ionic liquid electrolyte using a custom-made experimental setup (upper left in Fig. 2b) and were able to observe that the SEI layer exerted significant influences on lithium-ion diffusion and overall capacity of the single-nanobelt (NB) battery. Tsuda et al. [136] also observed SEI formation on silicon electrodes in [C_2mim][FSA] with Li[TFSA] and [C_2mim][TFSA] with Li[TFSA] electrolytes and reported that the in situ SEM observations revealed nonuniform darker deposits in comparison with those of other ionic liquid electrolytes, which suggested lower atomic numbers of the SEI constituents. And based on these observations of the contrast change during the electrochemical

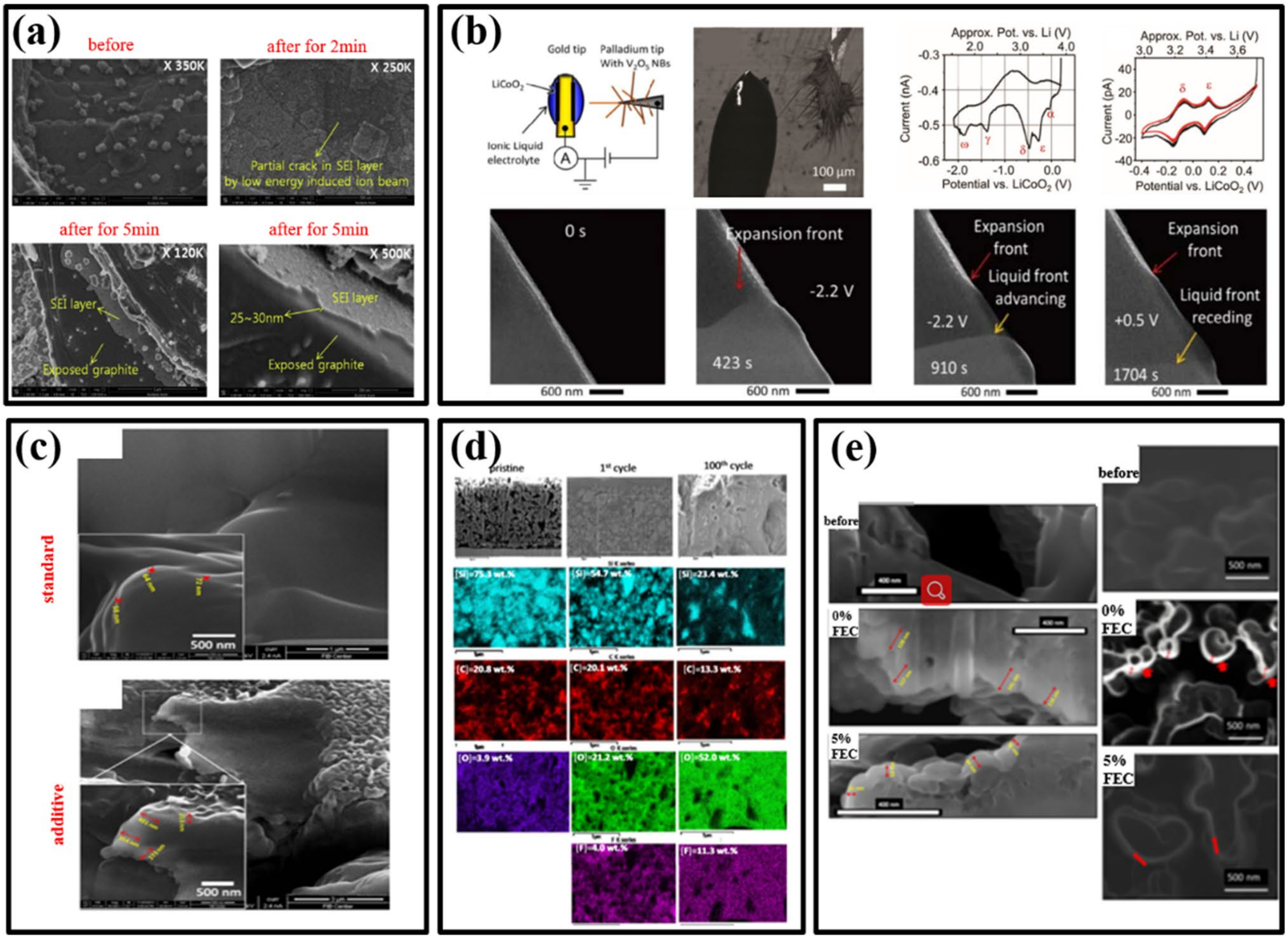

Fig. 2 In situ and ex situ SEM for SEI morphology observations. **a** XHR-SEM images of SEI layers on graphite electrodes before and after etching for 2 or 5 min. Reproduced with permission from Ref [34]. Copyright 2013, Elsevier. **b** The figures on the top row are the experimental setup, an SEM micrograph of a V_2O_5 whisker embedded in an electrolyte and cyclic voltammograms of two single-whisker battery devices; the figures on the bottom row from left to right are the in situ morphological changes during SEI formation. Reproduced with permission from Ref [35]. Copyright 2015, The Royal Society of Chemistry. **c** Cross-sectional FIB-SEM images of graphite electrodes after cycling in full cells with a standard electrolyte (top) and with transition metal salts added into the electrolyte (bottom). Reproduced with permission from Ref. [144]. Copyright 2014, The Electrochemical Society. **d** EDX maps of Si, C, O and F elements on FIB ablated cross sections of pristine, the first-cycle and the 100th-cycle electrodes. Reproduced with permission from Ref. [145]. Copyright 2016, The Electrochemical Society. **e** The images in the left column show FIB-SEM cross-sectional images of Si/graphene anodes in an EC/DEC (1:1, in weight ratios) electrolyte before and after 50 cycles from the discharged pouch full cells with 0% and 5 wt% FEC additives. The images in the right column show corresponding ion beam surface images of the Si/graphene anodes. Reproduced with permission from Ref. [36]. Copyright 2014, Elsevier

reaction, these researchers concluded that SEI formation can be suppressed in selected ionic liquid electrolytes.

To obtain more detailed information on SEI morphology, the focused ion beam (FIB) technique can also be used to prepare cross-sectional SEM samples. For example, Zhang et al. [143] were the first to apply FIB-SEM to the SEI research of a natural graphite sphere in an electrolyte composed of 1.0 M $LiPF_6$ dissolved in EC/DMC (1:1, in volume ratios). Here, these researchers reported that the SEI film also formed around cracks inside the natural graphite spheres and was relatively stable once formed with its thickness not increasing significantly during cycling. Following this study, numerous studies followed up on use of the FIB-SEM method [36, 144–149]. For example, Joshi et al. [144] investigated the effects of transition metal dissolution on the properties of the SEI layer in a graphite‖$Li_{1.05}Ni_{1/3}Co_{1/3}Mn_{1/3}O_2$ full cell with an electrolyte composed of 1.0 M $LiPF_6$ dissolved in EC/DEC (1:1, in weight ratios) with or without $Ni(TFSI)_2$, $Co(TFSI)_2$ and $Mn(TFSI)_2$ as additives and observed that the addition of transition metal ions into the electrolyte accelerated the growth of the SEI layer on the graphite anode into an irregular and much thicker film (Fig. 2c), thus explaining the cause of capacity and power attenuation in LIBs by using transition metal oxides as positive electrodes. In another study, Etiemble et al. [145] employed FIB-SEM to study SEI evolution on a silicon anode before and after 1, 10 and 100 cycles and reported that the silicon anode was progressively filled with SEI layers during cycling (Fig. 2d) and attributed this to the continuous accumulation of insoluble electrolyte degradation products, confirming the essential need to develop more effective electrolyte formulas to prevent excessive SEI formation to obtain viable Si-based electrodes. Bordes et al. [36] also investigated the effects of FEC additives on the capacity fading of full cells employing a Si/graphene anode and a NCA cathode and reported that optimized cell performances can be obtained at the FEC content of 5 wt%, which may be a result of the much thinner and more uniform SEI layer formed on the electrode as compared with other contents (Fig. 2e).

3.2.2 Morphological Characterization by TEM

TEM can provide much higher spatial resolution than SEM, and TEM-based electron energy loss spectroscopy (EELS) can examine chemical elements and valence states on imaged areas. However, the electron beams used in TEM can degrade electrolytes and SEIs, which is a problem that needs to be avoided. And similar to SEM, in situ TEM studies can also be carried out by using special liquid cells or IL electrolytes. Here, in situ TEM electrochemical cells can be divided into closed cells [150–152] and open cells [153, 154] in which in an open-cell configuration, the two electrodes are usually connected to a potentiostat and remain open in the TEM vacuum chamber, thus requiring the electrolyte used in these cells to be either solid electrolytes or ILs. As for closed-cell configurations, the entire electrochemical device is encapsulated in a thin flow-through liquid device with electronically transparent windows composed of materials such as silicon nitride (SiN_x). In addition, closed-cell configurations are typically designed on microfabricated silicon wafers with nanoscaled channels for the continuous flow of ordinary battery electrolytes. Furthermore, because the high vacuum of the TEM chamber is isolated from the liquid cell and has no effect on batteries, most common liquid electrolytes of LIBs can be used in these cells for in situ and in operando TEM investigations. As a result, the design of in situ TEM liquid cells opens up a wide field of application not only in battery materials, but also in other basic research of nanotechnologies.

In situ TEM has been used to investigate the SEI morphology of various electrode materials in LIBs, including carbon, silicon and alloying anodes as well as Li_xMO_y cathodes (M: Co, Mn, Ni and binary or ternary mixtures of transition metals) [37–39, 150, 155–163]. For example, Unocic et al. [150] studied SEI formation on glassy carbon electrodes in a $LiPF_6$/(EC + DMC) electrolyte using in situ electrochemical TEM (in situ EC-TEM) and were able to identity SEI constituents (such as LiF and Li_2CO_3) and lithium deposited on the glassy carbon through contrast changes in dark and bright-field imaging due to mass density differences. Furthermore, researchers have also used EELS analysis to reveal that SEI composition can include Li_2O, LiOH and LiF [164] in which the confirmation of LiF was consistent with the results observed in the graphite SEI by Wang et al. [165] using ex situ TEM–EELS.

Liao et al. [37] also investigated the cycling stability of a graphite‖$LiNi_{0.5}Co_{0.2}Mn_{0.3}O_2$ cell with electrolytes of 1.0 M $LiPF_6$ in EC + EMC (1:2, in weight ratios) with or without LiDFBOP additives at low temperature and found that cell performances in the LiDFBOP-containing electrolyte were significantly better. Here, the researchers attributed this performance difference to the serious electrolyte decomposition of the LiDFBOP-free electrolyte, which can result in a thick SEI layer covering the electrodes (especially the graphite anode) (Fig. 3a, b). Alternatively, LiDFBOP can be preferentially oxidized or reduced into bulk electrolyte components in the LiDFBOP-containing electrolyte to construct protective interface films on both the graphite anode and the $LiNi_{0.5}Co_{0.2}Mn_{0.3}O_2$ cathode, resulting in a homogeneous film that can not only inhibit electrolyte decomposition, but also exhibit high ionic conductivity due to the introduction of Li^+ from LiDFBOP into the films.

Silicon as an anode material can exhibit a specific capacity (4200 mAh g^{-1}) that is even higher than that of metallic lithium; however, Si experiences significant volume change of over ~ 300% upon alloying with lithium, resulting in significant issues including unstable SEIs. Therefore, the understanding of the formation and evolution of SEIs on Si anodes is important. And although initial SEI formation has rarely been observed on Si surfaces, Liu et al. [38] were able to observe nanometer-thick lithiation interfaces using TEM in which a 1-nm-thick interface between c-Si and a-Li$_x$Si [named as the amorphous crystalline interface (ACI)] was identified (Fig. 3c). Here, the researchers found that as the ACI moved toward the core of the c-Si wire, the a-Li$_x$Si increasingly thickened. In addition, the migration of the ACI was found to control lithiation kinetics in the Si nanowire without changing its thickness. In another study, Yuk et al. [162] studied the SEI on Si nanoparticles in a LiPF$_6$/(EC + DMC + DEC) electrolyte of a graphene liquid cell using TEM and reported that although the electron beam induced lithium accumulation around Si nanoparticles, lithiation preferentially started in the [110] direction of the Si particle. In addition, isotropic Li diffusion and anisotropic volume expansion were visualized in this study in which obtained EDS patterns showed the presence of high concentrations of C, O, P and F over the Si nanoparticles due to the SEI layer formation. Furthermore, these researchers also used selected-area electron diffraction to confirm the presence of LiF in this SEI layer.

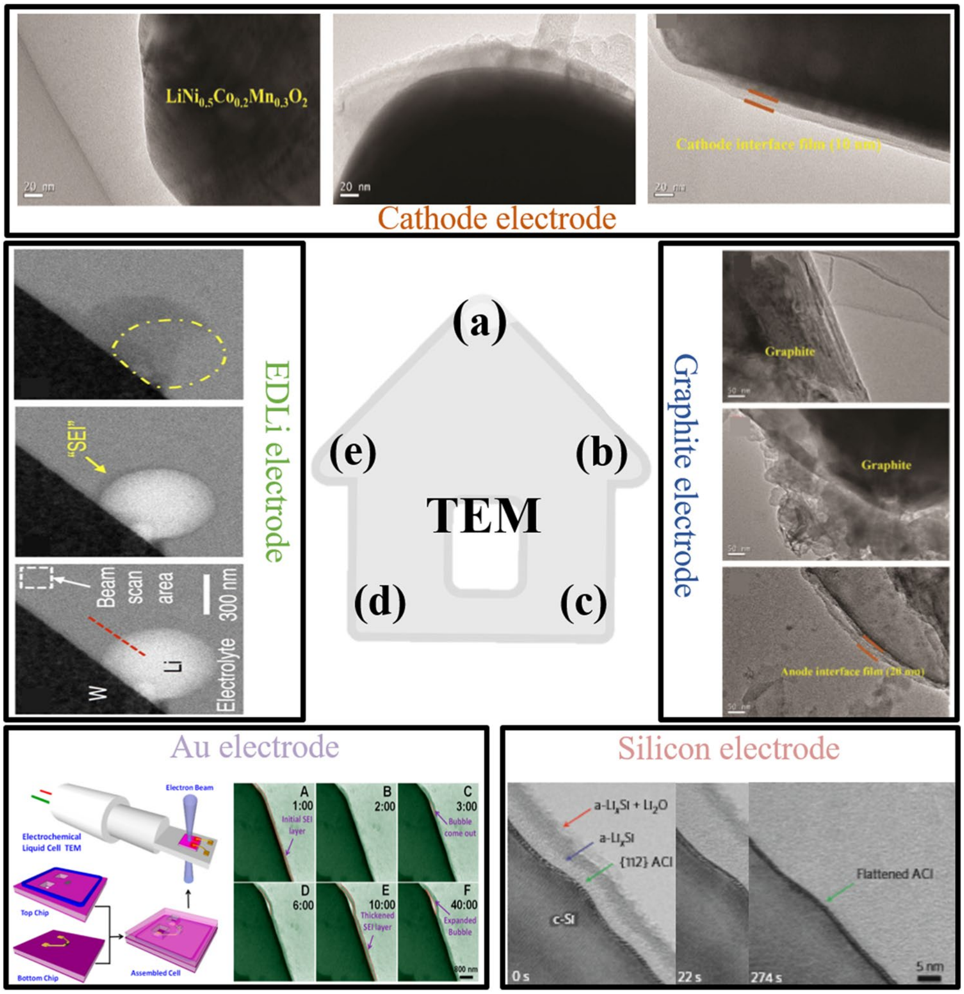

Fig. 3 Morphology observations of SEIs on various electrodes by using TEM. **a** TEM images of LiNi$_{0.5}$Co$_{0.2}$Mn$_{0.3}$O$_2$ cathodes from left to right: fresh, cycled at 0 °C and LiDFBOP-containing electrolytes. Reproduced with permission from Ref. [37]. Copyright 2018, John Wiley and Sons. **b** TEM images of graphite electrodes from top: fresh, cycled at 0 °C and cycled in LiDFBOP-containing electrolytes. Reproduced with permission from Ref. [37]. Copyright 2018, John Wiley and Sons. **c** Delayed images of {112} ACI migration in the lithiation process on a silicon electrode. Reproduced with permission from Ref. [38]. Copyright 2012, Springer Nature. **d** In situ TEM observations of the electrochemical reaction by using an electrochemical liquid cell (left) and SEI formation on Au electrode/liquid electrolyte interfaces (right). Reproduced with permission from Ref. [159]. Copyright 2014, American Chemical Society. **e** Beam-induced SEI growth on the surface of Li deposits and at the expense of Li stripping. Reproduced with permission from Ref. [160]. Copyright 2015, American Chemical Society

Moreover, Zeng et al. [159] used in situ TEM to investigate SEI formation on Au surfaces as an example of alloying materials and found that SEI thicknesses increased with increasing Au electrode volumes due to Li alloying with Au in which after a certain thickness, gas bubble formations on Au surfaces were observed, which subsequently can be peeled off from the SEI (Fig. 3d), demonstrating that Au is unsuitable as current collectors for LIBs due to its alloying nature and its catalytic reactions with lithium and battery electrolytes. Sacci et al. [157] also observed SEI growth during lithium electrodeposition on Au electrodes in a $LiPF_6$/(EC + DMC) electrolyte using in situ TEM and found that dendrite-shaped SEIs can form on Au electrode surfaces prior to Li electrodeposition and remain stable even after lithium dissolution. In addition, these researchers also found that the electrodeposition of Li also occurred through the SEI, which forms small nanoparticles within the SEI, suggesting that the entangled lithium particles in the SEI matrix can lead to dendrite formation.

Furthermore, the effects of electron beams in in situ TEM on electrolytes during cycling were also studied by Leenheer et al. [160] in a 1.0 M $LiPF_6$/EC + DMC (1:1) electrolyte on electrodeposited metallic lithium. Here, the researchers reported beam-induced SEI growth if beam scanning occurred near a growing Li deposit (Fig. 3e) in which a dark deposit formed and grew on the side of the Li grain closer to the beam exposure. In addition, these researchers also found that with increased beam exposure for 5 min, Li was electrochemically stripped, but the dark deposit remained and continued to grow. Moreover, the bright-field scanning transmission electron microscopy (BF STEM) contrast in the SEI became lighter than the electrolyte as beam scanning time increased, indicating that beam-induced SEIs may consist of chemical components such as LiF that can be reduced back to metallic Li.

3.2.3 Morphological Characterization by AFM

AFM can provide nanometer-scaled spatial resolution and versatile imaging environments for morphological characterizations. In addition, AFM can be used on a variety of samples including insulating materials, and because this technique does not use beams (electron or optical) or lenses, it can operate in liquid environments. Furthermore, its high-magnification imaging allows for the monitoring of nanoparticles in electrochemical reactions in which the constant repulsion contact force between the tip and the specimen is used to scan the surface morphology of specimens. However, AFM requires relatively flat sample surfaces to achieve stable and good-quality images.

Highly oriented pyrolytic graphite (HOPG) is a commonly used graphite anode model in AFM-based LIB studies. For example, Deng et al. [166] reported that for HOPG cycled in a LiTFSI/DEC electrolyte, SEI formation started at 1.45 V versus Li/Li^+ on electrode surface defects but that the surface of HOPG carbon was not completely covered by ring-like SEIs and that the SEI thickness remained at 10.4 ± 0.2 nm in the first cycle. However, these researchers also reported that in the following cycle, the surface of HOPG carbon became completely covered (Fig. 4a). Jeong et al. [167] further studied SEI films on the basal plane of HOPG in a $LiClO_4$/(EC + DEC) electrolyte using in situ AFM and proposed two types of SEI morphology, including a hill-like 1–2-nm-tall structure and a blister-like structure with a large swelling of heights to 5–20 nm in which the appearance of the latter morphology in the potential range of 1.0–0.8 V confirmed the intercalation of solvated Li^+. And at potentials below 0.65 V, particle-like precipitates appeared on the basal plane, which were also observed by Alliata et al. [168] in their study, indicating that electrolyte breakdown was easier in this potential range and resulted in these granular structures. Furthermore, Jeong et al. [167] also reported that the thickness of the SEI in the first cycle was ~ 40 nm and increased to 70 nm in the second cycle, confirming that SEI formation is a dynamic process. Moreover, Novak et al. [169] also investigated the dynamic process of SEI growth on a carbon electrode in a $LiPF_6$/(EC + DMC) electrolyte and found that the changes in the surface profiles started at ~ 0.7 V and that an SEI with a thickness of 15 nm formed after reaching 0.25 V versus Li/Li^+ (Fig. 4b). And at the end of the second charge/discharge cycle, a uniform SEI with a thickness of 20 nm formed, indicating the completion of SEI growth.

Effects of temperature, lithium salts and film-forming additives on SEI formation can also be investigated on carbon-based anodes by using in situ AFM [170–179]. For example, Edstrom et al. [170] observed the formation of a ~ 5-nm-thick SEI at 0.8 V using in situ AFM in a $LiBF_4$/(EC + γ-BL) electrolyte but reported that as temperatures reached 50 °C or above, the formed SEI cracked, leading to the exposure of fresh HOPG carbon surfaces to the electrolyte. Koltypin et al. [171] also investigated the effects of anions in lithium salts on SEI morphology through the in situ AFM observation of SEI growth on HOPG in $LiPF_6$ and $LiAsF_6$ (in EC + DMC) electrolytes and found that in the case of $LiPF_6$ salt, the SEI surface morphology was compact with fine grains, whereas in the case of $LiAsF_6$ salt, it was smooth and smeared. In addition, Morigaki et al. [174] used in situ AFM to find that SEI morphology was dependent on lithium salts of electrolytes and proposed that differences in SEI chemistry can result in different SEI structures. Furthermore, researchers have also reported that electrolyte salt concentrations can significantly influence interfacial structures in which Liu et al. [172] reported that concentrated electrolytes with molar ratios (Li:DMSO) of 1:2 or 1:3 enabled SEI formation on HOPG edges to effectively stop the

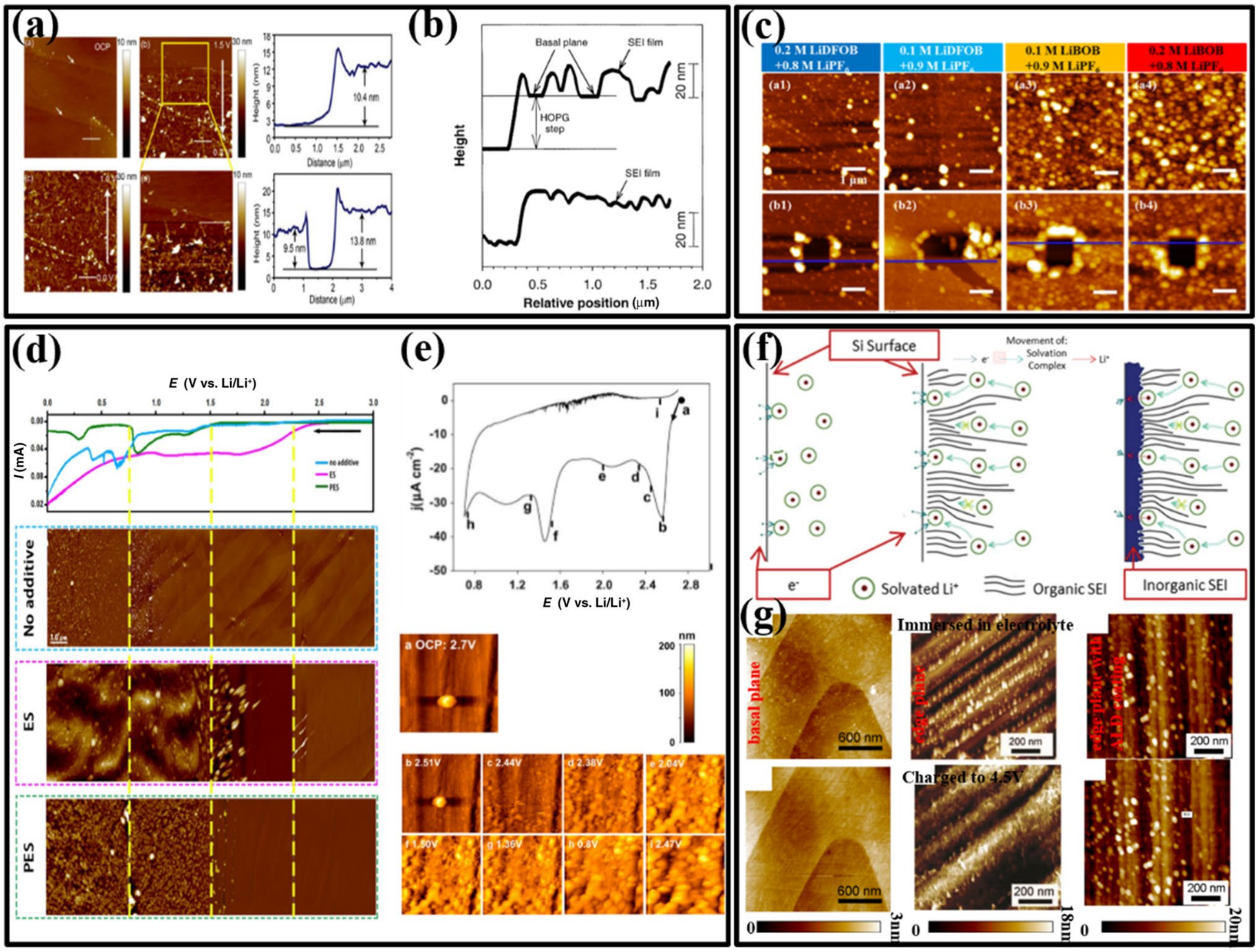

Fig. 4 Morphology observations of SEIs on various electrodes and electrolytes by using in situ and ex situ AFM. **a** In situ AFM images of an HOPG electrode at open-circuit potential and continuous potential scanning. The arrow indicates the direction of voltage and the scan. Reproduced with permission from Ref. [166]. Copyright 2013, Science China Press and Springer-Verlag Berlin Heidelberg. **b** Vertical surface profiles of an SEI protective film formed on an HOPG electrode obtained by in situ AFM. Reproduced with permission from Ref. [169]. Copyright 2001, Elsevier. **c** AFM images of SEI layers formed on HOPG electrodes in various electrolytes after the first CV cycle. Reproduced with permission from Ref. [175]. Copyright 2018, Elsevier. **d** AFM images of the in situ monitoring of freshly cleaved HOPG electrodes in 1.0 M $LiPF_6$/(EC + DMC) electrolytes with no additives, 1 wt% ES and 1 wt% PES, and their corresponding voltammetry. Reproduced with permission from Ref. [189]. Copyright 2013, The Royal Society of Chemistry. **e** In situ AFM images of Sn-foil anodes in 1.0 M $LiPF_6$/(EC + DEC) (1:2, in weight ratios) electrolytes recorded at various potentials. Reproduced with permission from Ref. [40]. Copyright 2009, Elsevier. **f** SEI growth model proposed by in situ AFM on a Si anode in a $LiPF_6$/(EC + DMC) electrolyte. Reproduced with permission from Ref. [180]. Copyright 2014, American Chemical Society. **g** In situ formation and imaging of CEI film formation and decomposition on different planes of $LiCoO_2$ with or without ALD coating crystals at different states. Reproduced with permission from Ref. [184]. Copyright 2017, American Chemical Society

co-intercalation of solvated Li^+ in graphite lattices, whereas diluted electrolytes with a molar ratio of 1:4 enabled SEI formation at the basal plane, which cannot stop the co-intercalation of solvated Li^+. Furthermore, Huang et al. [175] studied the SEI on HOPG cycled in electrolytes with lithium difluoro(oxalate)borate (LiDFOB) and LiBOB additives and reported that after the first CV cycle, the particle sizes on the SEI film in the LiBOB-containing electrolyte were much bigger than those formed in the LiDFOB-containing electrolyte (Fig. 4c). And based on the thickness of the SEI layers formed in four different electrolytes (0.2 M LiDFOB + 0.8 M $LiFP_6$, 0.1 M LiDFOB + 0.9 M $LiFP_6$, 0.2 M LiBOB + 0.8 M $LiFP_6$ and 0.2 M LiBOB + 0.8 M $LiFP_6$), these researchers concluded that increasing amounts of LiDFOB additives in the electrolyte can lead to thinner SEI films, whereas increasing amounts of LiBOB can lead to thicker SEI films, suggesting that the decomposition of LiBOB additives was more intense than LiDFOB additives.

The effects of solvent additives such as ethylene sulfite (ES) and prop-1-ene-1,3-sultone (PES) on SEI formation were also investigated by Lin et al. [176] by using in situ AFM. Here, the researchers observed SEI film formation on HOPG in different electrolytes (1.0 M $LiPF_6$/EC + DMC, 1.0 M $LiPF_6$/EC + DMC and 1.0 M $LiPF_6$/EC + DMC + 1%PES) and reported that the reduction potentials of ES and PES to form SEI layers were higher than those in the baseline electrolyte (Fig. 4d) and that the initial particle sizes in the SEI layer formed with the ES additive were in the range of 40–60 nm with the lateral dimension of the particles being ~ 500 nm, which were much larger than those formed with the PES additive. These researchers subsequently combined TEM results with these in situ AFM results and concluded that the SEI layer formed in the ES-containing electrolyte was thicker and denser than that formed in the PES-containing electrolyte, possibly explaining the enhanced battery performance as promoted by ES additives.

Sn and Si can both be used as high-capacity anode materials for LIBs; however, they both experience significant volumetric change along with instability of the passivation film during battery cycling, resulting in large irreversible capacity losses and low CEs and inhibiting application in LIBs. To address these issues, the understanding and modification of surface film stability on these electrodes are required. Based on this, Lucas et al. [40] investigated SEI formation on Sn electrodes in 1.0 M $LiPF_6$/EC + DEC (1:2, in weight ratios) electrolytes using in situ AFM and found that at the first CV scan starting from OCP to ~ 0.7 V, SEI formation started at ~ 2.5 V and that between the range of 2.5 V to ~ 2 V, the SEI layer grew rapidly to form a 100–150 nm rough film consisting of micron-sized platelets (Fig. 4e). In addition, these researchers also found that if the voltage decreased below 2 V, the SEI layer changed to a porous membrane surface composed of larger particles. And by comparing the morphology of the SEIs formed at different potentials and the CV results, these researchers suggested the existence of an overlayer on the SEI film that may dissolve in the electrolyte. In addition, these researchers also observed rougher SEI reformation in the subsequent two cycles, indicating that the SEI layer was unstable and that optimizations to form stable surface films were needed.

In another study, Tokranov et al. [180] investigated the initial process of SEI formation on Si anodes under various conditions in a 1.0 M $LiPF_6$/EC + DMC (1:2, in volume ratios) electrolyte using in situ AFM and found that the rapidly formed initial SEI can be stabilized before significant Li alloying with Si and that the rate at which this occurred varied significantly with the nature of the electrode (bare Cu, bare Si, Al_2O_3-coated Si). In addition, these researchers reported that the initial cycling conditions also had a substantial impact on SEI morphology, with faster current rates leading to smoother, thinner SEI films. And based on these results, these researchers proposed the so-called multilayered SEI model (Fig. 4f).

Compared with anode materials, cathode materials usually exhibit less volume expansion during cycling. In addition, typical electrolytes are stable at cathodes up to ~ 4.20 V. Nevertheless, CEIs can still form on cathodes and are as important as SEI formation, especially in high-voltage LIBs. Therefore, increasing investigations on CEIs through AFM have been conducted [128, 181–188]. For example, Li et al. [181] investigated the morphology evolution of the CEI formed on a $LiNi_{0.5}Mn_{1.5}O_4$ (LNMO) cathode in a $LiPF_6$/(EC + DMC + EMC) electrolyte in the first charge/discharge cycle and found that on the LNMO surface, precipitates started to appear if the battery was charged to 4.65 V due to the oxidative decomposition of the electrolyte components. These researchers also reported that if the battery further charged to 4.75 and 4.95 V, the precipitates increased significantly, whereas during discharge back to 4.65, 4.20 and 3.20 V, the precipitates partially decomposed, indicating the instability of the CEI at high-voltage cycles. Lu et al. [184] also investigated CEI formation on layered $LiCoO_2$ microcrystals (another commonly used cathode material) in a $LiPF_6$/(EC + DMC + EMC) electrolyte in high-voltage cycling and reported that the in situ AFM results showed different CEI morphology evolution behaviors on the basal plane versus the edge plane, with or without thin ALD coatings (Fig. 4g). Here, these researchers found that CEI films with loose fibrillar structures formed on the edge planes of $LiCoO_2$ microcrystals if charged to 4.5 V and were unstable and decomposed at lower voltages, whereas CEIs were not observed on the basal planes or edge planes with a thin ALD coating of Al_2O_3, suggesting that cobalt ions exposed on edge planes can catalyze the oxidative decomposition of electrolytes. And overall, these results indicated that the high-voltage cycling stability of $LiCoO_2$ and related layered cathode materials can be improved through the regulation of surface compositions.

3.3 Compositional Characterization Techniques

3.3.1 Fourier Transform Infrared Spectroscopy (FTIR)

FTIR is a vibrational spectroscopy technique that is widely used in chemistry to identify functional groups and chemical structures [190]. And in SEI research, FTIR has become a powerful tool to track chemical changes in electrolyte/electrode interfaces. For example, Aurbach et al. [191] first used ex situ FTIR to monitor SEI formation and degradation on metal electrodes (Au, Pt, Ag) in lithium salt solutions in γ-butyrolactone (BL). Here, these researchers found that BL can reduce to carboxylates on metal electrode surfaces, whereas the oxygen-containing solution showed typical carboxylate moiety (Fig. 5a) and that as these compounds

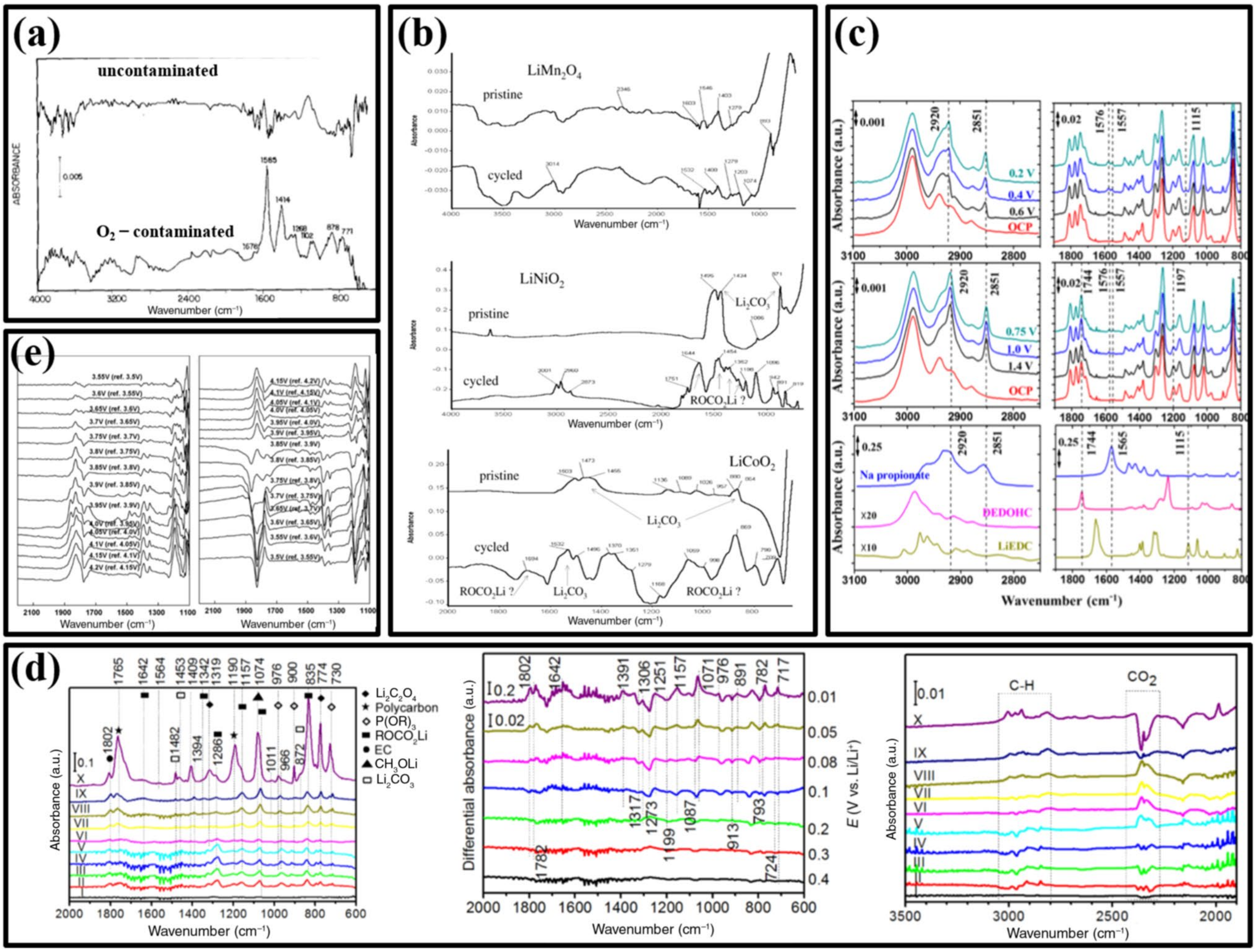

Fig. 5 In situ and ex situ FTIR for the chemical composition analyses of SEIs. **a** FTIR spectra obtained from uncontaminated and O_2-contaminated solutions. Reproduced with permission from Ref. [191]. Copyright 1989, The Electrochemical Society. **b** FTIR spectra obtained from pristine and cycled composite $LiMn_2O_4$, $LiCoO_2$ and $LiNiO_2$ electrodes. Reproduced with permission from Ref. [192]. Copyright 2003, Elsevier. **c** Au (top) and Sn (middle) electrodes obtained at various potentials and ATR-FTIR spectra of sodium propionate, DEDOHC and LiEDC (bottom). Reproduced with permission from Ref. [45]. Copyright 2015, American Chemical Society. **d** From left to right: difference FTIR spectra at 0.8 V in the lithium removal process, in situ infrared spectra of silicon-powder electrodes at different potentials and in situ FTIR spectra in the wave number region of 1900–3500 cm^{-1}. Reproduced with permission from Ref. [203]. Copyright 2016, John Wiley and Sons. **e** In situ PM-FTIR spectra of $LiCoO_2$ films in the CV scanning of PC-containing electrolytes. Reproduced with permission from Ref. [204]. Copyright 2007, Elsevier

reacted further, SEIs can form with the solvent nucleophilically. Aurbach et al. [192] also summarized the chemical composition characterizations of SEIs/CEIs on various carbon electrodes (graphite, hard and soft disordered carbons, carbon nanotube electrodes) and several commonly used cathode materials ($LiNiO_2$, $LiCoO_2$ and $LiMn_2O_4$) using ex situ FTIR in which for carbon particles, the initial species found during the first cathodic polarization were oxygen-containing groups on the surface (i.e., OH, COOH, C = O, which can be reduced to –OLi, –COOLi, etc.). However, these researchers also found that the dominant components in the SEI were dependent on the electrolyte. Here, these researchers reported that if electrolytes did not generate HF [solutions of $LiClO_4$, $LiAsF_6$, $LiN(SO_2CF_3)_2$, $LiN(SO_2CF_2CF_3)_2$], SEI chemistries were controlled by solvent reduction processes. Therefore, in alkyl carbonate solvents, major SEI components were $R(OCO_2Li)_2$ (reduction products of EC, PC), $ROCO_2Li$ and ROLi (reduction products of DMC, EMC, etc.) and Li_2CO_3 (a reaction product of trace H_2O with $ROCO_2Li$). And in cases in which electrolytes can generate the high HF content (e.g., in $LiPF_6$ solutions at high electrolyte/electrode ratios and conditions for hydrolysis), the SEI was dominated by LiF and ROLi due to the removal of $ROCO_2Li$ from the surface due to their reaction with HF. And for the above-mentioned cathode materials in electrolytes of $LiPF_6$ dissolved in EC + DMC mixtures, these researchers concluded that the surfaces of $LiNiO_2$ and $LiCoO_2$ particles are more nucleophilic and basic than $LiMn_2O_4$ and therefore can react more readily with solution species (nucleophilically with alkyl carbonates and as bases with HF, Fig. 5b).

To overcome intense masking effects of solvent IR bands, special electrochemical cells with IR transparent windows have been designed to enable in situ FTIR measurements [99, 193–196]. In addition, the existence of similar functionalities between electrolytes and SEI components can result in overlapping peaks, making the identification of chemical species difficult. To address this, various IR modes such as attenuated total reflectance (ATR), photoacoustic IR, diffused reflectance IR, subtractive normalized interfacial FTIR (SNIFTIR), transmission IR, near-normal incidence reflectance, grazing incidence reflectance and double-modulation IR have been used to monitor the in situ chemical composition evolution of SEIs/CEIs [197–200]. For example, Pyun et al. [198] used in situ ATR-FTIR to accurately monitor SEI components in two different electrolytes of $LiPF_6$ and $LiAsF_6$ dissolved in EC/DEC and found that $LiPF_6$ was less reductive than $LiAsF_6$ in electrochemical cycling and that the $ROCO_2$, Li_2CO_3, Li_xPF_y and Li_xAsF_y in the SEI originated from the reduction of solvents and lithium salt. Winter et al. [199] also monitored SEI formation in chloroethylene carbonate (ClEC) and $LiN(SO_2CF_3)_2$ in EC using in situ SNI-FTIR and found that CO_2 formation assisting in SEI formation only existed in ClEC. In addition, Lanz et al. [200] found that the SEI formed on graphite in $LiClO_4$/(EC + DMC) electrolytes was composed of various organic/inorganic species such as $(CH_2OCO_2Li)_2$, alkyl(di)lithium carbonate and Li_2CO_3 using FTIR and Hongyou et al. [201] studied the role of VC additives in $LiClO_4$/(EC + DMC) electrolytes on graphite surfaces using in situ FTIR. Here, the obtained results showed that the formation of lithium alkyl carbonate was reduced by VC, indicating the suppression of EC decomposition and demonstrating that VC can play a crucial role in the protection of electrolytes from decomposition. Furthermore, other additives such as ES, benzyl isocyanate (BIC) and 4-bromobenzyl isocyanate (Br-BIC) in PC-based electrolytes have also been found to be capable of preventing PC solvent decomposition by using FTIR [202].

Compared with graphite anodes, lithium metal and alloy anodes possess higher energy densities and are regarded as promising anode materials for next-generation lithium batteries. However, lithium metal is highly reactive toward electrolytes. As a result, researchers have applied FTIR techniques to investigate the SEI characteristics of these highly reactive lithium-based electrodes. For example, Morigaki et al. [174] used in situ FTIR to show that in $LiPF_6$/(EC + DMC) electrolytes, EC and DMC can be reduced to lithium alkyl carbonate after the immersion of a lithium metal electrode into the $LiPF_6$/(EC + DMC) electrolyte for 15 h. In addition, these researchers also found that if the lithium metal electrode was soaked in the electrolyte for longer time, CO_2 peak intensities increased and solvent peak intensities decreased in the FTIR spectra, confirming the reduction of EC into $ROCO_2Li$ and CO_2. In another study, Shi et al. [45] used in situ ATR-FTIR analysis to study SEI formation on Sn and Au electrodes in a $LiPF_6$/(EC + DEC) electrolyte and reported that both electrodes possessed lithium propionate as a common SEI constituent, but that the SEI on the Sn electrode contained diethyl 2, 5-dioxahexane dicarboxylate (DEDOHC), whereas the SEI on the Au electrode contained lithium ethylene dicarbonate (LiDEC). Here, the researchers proposed that the mechanism of SEI formation involved the strong interaction between the Sn surface and the solvent (mainly DEC) due to surface oxygens, which led to the formation of ethyl oxide. This ethyl oxide radical can subsequently serve as an intermediate to further decompose EC to form DEDOHC (Fig. 5c).

Yang et al. [203] also used in situ FTIR to investigate SEI formation on Si electrodes in a $LiPF_6$/(EC + DMC) electrolyte and found that SEI formation over Si electrodes started at 0.87 V (Fig. 5d). In addition, these results revealed that SEI thicknesses increased and lithium alkyl carbonates started to appear as Si electrodes polarized toward lower potentials. This large volume expansion during the alloying of Si subsequently led to the breakage of the SEI layer and the exposure of fresh Si surfaces. And as a result, substantial electrolyte decomposition occurred during de-lithiation. In addition, degradation of the electrolyte salt $LiPF_6$, starts during de-lithiation leading to the decomposition of lithium alkyl carbonate through reactions with HF and free radicals or Li, resulting in the formation of alkyl phosphate and Li_2CO_3. Furthermore, these researchers reported that de-lithiation can also lead to the formation of organic components such as lithium oxalate and lithium alkyl carbonates, thus suggesting that more SEI components are formed during de-lithiation than lithiation.

The CEI on cathode materials has also been frequently studied by using in situ FTIR. For example, Matsui et al. [204] investigated the electrochemical oxidation behaviors of $LiClO_4$/(EC + DEC) and $LiClO_4$/PC electrolytes with a $LiCoO_2$ cathode using in situ FTIR and found that the solvents and salts both degraded during the discharge process and that this degradation resulted in the deposition of Li_2CO_3 and poly-oxyethylene to form a surface film that was unstable and stripped out during cathodic polarization (Fig. 5e). In addition, these researchers found that because the oxidized species were only weakly adhered to the $LiCoO_2$ surface, the deposition and stripping process continued for a few cycles until the interfacial film reached a certain thickness so that no electrons could penetrate through. Subsequently, these researchers extended this experiment to $LiMn_2O_4$ and $LiNi_{1/2}Mn_{3/2}O_4$ cathodes and observed similar phenomena. And by combining the results of these three materials, these researchers suggested that electrolyte salts can decompose and form a layer of carboxylic derivatives, which can further decompose to form a complex CEI [205]. Matsui et al. [206] also investigated $LiCoO_2$ cathode interfaces in electrolytes of LiBOB/(EC + DEC), $LiPF_6$/(EC + DEC) and (LiBOB + $LiPF_6$)/(EC + DEC) using in situ FTIR and found that LiBOB preferred to adhere to cathode surfaces and that BOB^- anions could protect PF_6^- ions in $LiPF_6$ salts from decomposing into PF_5 and LiF, which prevented interface formation and therefore minimized electrolyte breakdown. Matsushita et al. [207] also studied CEIs on $LiCoO_2$ cathodes in PC-based electrolytes with various salts (i.e., $LiPF_6$, $LiBF_4$ and $LiClO_4$) using in situ FTIR and found that PC can oxidize into carboxylic-group-containing compounds and further convert into an anhydride form and remain on the electrode surface. These researchers also found that the above reactions of PC were influenced by the various salts and were more active in $LiPF_6$ salts as compared with the others.

3.3.2 X-ray Photoelectron Spectroscopy (XPS)

In XPS analysis, incident X-rays photons (typically Al $K\alpha = 1486.6$ eV, Mg $K\alpha = 1253.6$ eV) are absorbed by material surfaces and photoelectrons are ejected from the surface in which the energy spectra of these photoelectrons are analyzed with a detector. As a result, XPS is capable of analyzing almost all elements of the periodic table (except H and He) if their concentrations are > 0.1 at % of the material surface with energy resolution of 0.1 eV [208]. And although XPS is a surface analysis technique, it can also provide depth analysis in which a nondestructive method involves the adjustment of incident angles to tune the penetration depth of the X-rays (< ~10 nm), whereas a destructive method involves the etching of sample surfaces by several hundred nanometers with a sputtering ion gun. Here, both methods can be useful for SEI/CEI studies; however, due to the electronically insulating nature of SEIs/CEIs, the charging up of samples due to the ejection of photoelectrons needs to be carefully avoided in XPS measurements. In addition, special liquid electrolyte cells or special instrument designs are required for in situ XPS studies on SEIs/CEIs because an ultrahigh-vacuum ($< 10^{-8}$ Pa) environment is necessary for the energy analyzer.

For example, Malmgren et al. [42] investigated chemical composition differences between SEIs on lithiated graphite anodes and CEIs on delithiated lithium iron phosphate cathodes using XPS and found that the inner layer of the SEI contained compounds such as lithium oxide and alkoxides that were not observed in the cathode CEI (Fig. 6a). Here, these researchers largely attributed these differences to the different electrochemical reactions at the operating potentials of the anode and the cathode. In addition, these researchers also found from their XPS results that the main components in the outer layer of the SEI were C–H- and C = O-containing compounds, which were also found to be the main components of the cathode CEI, and proposed that the similarities between the SEI outer layer and the CEI were associated with the dissolved portion of the electrolyte reduction products originating from the formation of the inner layer SEI on the anode. Furthermore, these researchers also conducted depth profile analysis by XPS and found that after a few cycles, the SEI thickness on the lithiated graphite anode was ~ 17 nm, whereas the CEI on the delithiated lithium iron phosphate cathode was estimated to be a few nanometers.

In another study, Chan et al. [41] studied SEI formation on a silicon nanowire anode in a $LiPF_6$/(EC + DEC) electrolyte using ex situ XPS and found that the chemical composition of the SEI was voltage dependent in which after the initial charge to 0.5 V, the SEI film was found to be composed of similar amounts of hydrocarbons, LiF, Li_xPF_y, $Li_xPF_yO_z$ and PEO-type oligomers, along with less amounts of ethers and lithium alkyl carbonates (Fig. 6b). And if the anode was further charged to 0.1 V, the SEI was found to be composed of mainly hydrocarbons and PEO-type oligomers, indicating the reduction of more electrolytes. Moreover, Li_2CO_3 was detected in the SEI at 0.1 V but ethers or lithium alkyl carbonates were not, indicating that these meta-stable components may have transformed into Li_2CO_3. Furthermore, the amounts of LiF and $LiPF_6$ in the SEI at 0.1 V were found to be lower than those at 0.5 V and that if fully charged to 10 mV, the SEI consisted mainly of stable Li_2CO_3 and LiF. In another study, Chen et al. [139] characterized the chemical components of the SEI formed on a Si film anode in $LiPF_6$/EC: DEC electrolytes with and without VC using ex situ XPS, and found that the existence of VC in the electrolyte decreased the LiF content in the SEI layer and improved the electrochemical performance of the Si film anode. In addition, Song et al. [209] investigated the effects of VC on the cycling performances of a graphite‖$LiFePO_4$ cell at elevated temperatures using ex situ XPS and based on their obtained results, suggested that the addition of VC can help to form a CEI layer on the cathode to suppress the dissolution of Fe from the $LiFePO_4$ cathode and improve the SEI stability on the anode.

Maibach et al. [210] proposed in situ XPS for SEI analysis in LIBs, and as a result, numerous in situ XPS studies have emerged [43, 44, 84, 211, 212]. For example, Park et al. [44] investigated the electrochemical performance of a Li‖$LiCoO_2$ cell in a 1.0 M $LiPF_6$/EC + DEC (1:1, in volume ratios) electrolyte with or without FEC additives using 2D correlation XPS for cathode materials and found that the 2D correlation spectra of the C1 s region obtained from the charged $LiCoO_2$ electrode in the FEC-free and

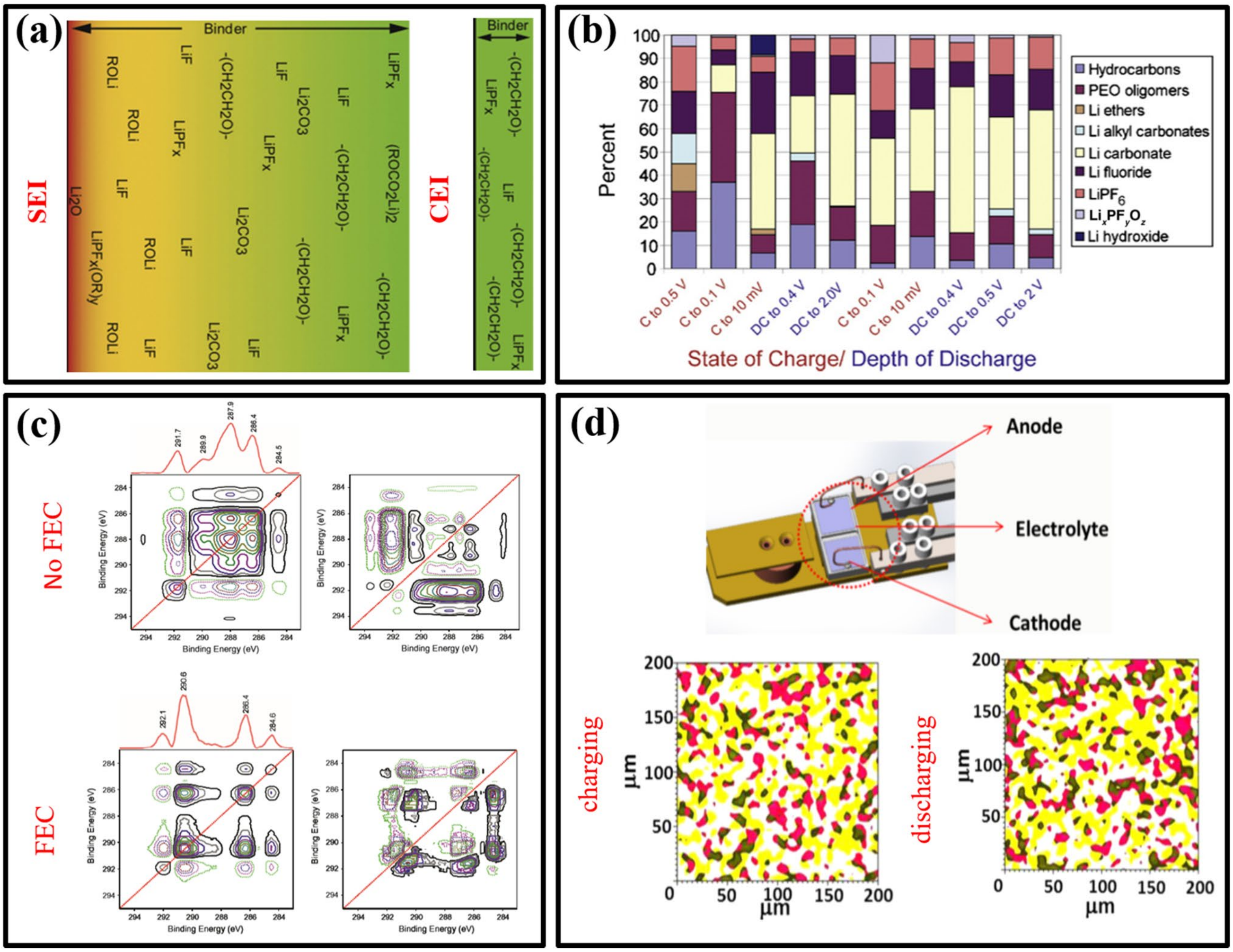

Fig. 6 In situ and ex situ XPS for the composition analysis of SEIs/CEIs on various electrodes. **a** Schematic of the SEI on a lithiated graphite anode and the CEI on a carbon-coated delithiated $LiFeO_4$ cathode. Reproduced with permission from Ref. [42]. Copyright 2013, Elsevier. **b** Molecular species found at different surface potentials of SiNW samples by using XPS high-resolution scanning. Reproduced with permission from Ref. [41] Copyright 2009, Elsevier. **c** Synchronized (left) and unsynchronized (right) 2D C1 s XPS spectra of $LiCoO_2$ particles during overcharging. Reproduced with permission from Ref. [44] Copyright 2014, Elsevier. **d** Diagram of a sample holder (top) for in situ XPS characterization and XPS chemical imaging of the lithium electrode–electrolyte interface after the first charge/discharge cycle (bottom right) and a picture representation of the SEI layer growth mechanism of Li–S batteries based on XPS and computational results (bottom left). Reproduced with permission from Ref. [43] Copyright 2017, American Chemical Society

FEC-containing electrolytes were different (Fig. 6c) and concluded that the PVDF binder and electrolyte components had decomposed to form a CEI on $LiCoO_2$ and that the addition of FEC increased the amount of polycarbonate, which became the dominant species in the CEI film. Nandasiri et al. [43] also investigated the evolution of SEI layers on lithium anodes within Li–S batteries using in situ XPS and found that the SEI layer evolution consisted of three major processes, including the formation of a primary composite containing stable lithium compounds (e.g., Li_2S, LiF, Li_2O), the formation of a secondary matrix as a result of cross-interactions between reaction products and electrolytes and a highly dynamic monoanionic polysulfide (i.e., LiS_5) fouling process (Fig. 6d). Recently, Tang et al. [211] also used in situ XPS and Auger electron spectroscopy to study the use of carbon-supported titanium grid current collectors and ionic-liquid-based electrolytes in which partially reversible conversions between Cu and CuO, and Li_2O formation were observed in a LiTFSI/P_{13}TFSI electrolyte against a Li counter electrode.

3.3.3 Secondary Ion Mass Spectrometry (SIMS)

Another technique for the chemical composition characterization of SEIs/CEIs is SIMS, which was developed by A. Benninghoven in 1970 [213]. In SIMS, ion beams typically in the energy range of 250–30 keV are applied to sputter sample surfaces to generate secondary ions, which are subsequently analyzed by using a mass spectrometer (often a time-of-flight (ToF) type) to obtain mass-to-charge (*m*/*z*) ratios of ions. As a result, SIMS can provide depth profiling of elemental compositions through ion etching. Furthermore, the mass resolution of SIMS is typically high enough to distinguish isotopes in which the static mode is frequently used to generate surface composition maps with lateral resolution of 5 nm and concentration sensitivities in the ppm level [214]. Alternatively, high-power-ion generating sources can be used in the dynamic mode to provide higher ion fluxes for in-depth profiling, allowing for the measurement of elemental concentrations down to the 10^{-9} (μg/L) level [215]. And by combining these two modes, 3D elemental mapping of material surfaces can be achieved and is known as 3D SIMS.

For example, Peled et al. [216] first employed ex situ SIMS to investigate elemental distribution within SEIs and studied the composition and thickness of SEIs over different planes (the basal plane and the edge plane) of HOPG. Here, the results revealed that the main constituents of the SEI at the edge plane were Li and F in inorganic form, whereas the main constituents of the SEI at the basal plane were mainly organic species. ToF–SIMS can also provide direct evidence for the presence of polymers in the basal plane. For example, Shi et al. [52] used ToF–SIMS to study Li-ion transportation through the SEI on a Cu electrode and proposed a two-layer/two-mechanism model for Li-ion diffusion in SEI films in which in 5-nm-thick porous organic SEI layers, Li^+ can diffuse extremely fast, whereas in dense inorganic SEI layers composed predominantly of crystalline Li_2CO_3, instead of direct hopping through empty spaces between Li_2CO_3 lattice sites, Li^+ diffused slowly through a repetitive knockoff with lattice Li-ion sites within the (100) surface of the Li_2CO_3 (Fig. 7a).

Pereira-Nabais et al. [217] also used ex situ ToF–SIMS and XPS to investigate the SEI on Si electrodes in distinct 1.0 M $LiClO_4$/PC and 1.0 M $LiPF_6$/EC + DMC electrolytes and found that the SEI film contained organic carbonate species in the outer layer and inorganic species in the inner layer in which a thicker SEI layer was formed in the 1.0 M $LiClO_4$/PC electrolyte as compared with that in the 1.0 M $LiPF_6$/EC + DMC electrolyte. In another study, Ota et al. [24] analyzed SEI formation on composite graphite and HOPG in a VC-containing electrolyte using ex situ ToF–SIMS and found that the SEI formed in the VC-containing electrolyte consisted of polymer components such as poly(VC), oligomers of VC and polyacetylene. In addition, $(CHOCO_2Li)_2$, $(CH{=}CHOCO_2Li)_2$, $(CH{=}CHOLi)_2$ and RCOOLi were also detected on the graphite surface as VC reduction products. These researchers also found that the reductive gases of the EC solvent (e.g., C_2H_4, CH_4 and CO) in the EC-based electrolyte can be suppressed with VC additives. Furthermore, VC additives were also found to be able to increase the thermal decomposition temperature of the SEI.

3.4 Recent Developments in Characterization Techniques

3.4.1 Depth Profiling by Using In Situ ToF–SIMS

The in situ application of SIMS in the study of LIBs remains challenging due to the high volatility of nonaqueous liquid electrolytes. To address this, Zhu et al. [53] designed an in situ cell for the analysis of lithium plating and stripping processes in a $LiPF_6$/(EC + DMC) electrolyte on a Cu electrode using ToF–SIMS. Here, the in situ cell consisted of a bottom piece with $LiCoO_2$ coated on an Al current collector as the lithium source and a top piece with a Cu film sputter-coated on a thin Si_3N_4 window (Fig. 7b). And with the cell filled with electrolytes, a Bi^+ ion beam was first used to punch through the Si_3N_4 window and the Cu film to form an extremely small orifice and subsequently was used as the primary ion beam for the ToF–SIMS analysis of the SEI that evolves at both the Li-metal surface and in the liquid electrolyte, allowing for the 3D mapping of concentration changes of different species generated by the breakdown of the electrolyte components (Fig. 7c). Here, the obtained 3D SIMS maps showed that as charging proceeded, Li^+ migrated to the anode (the Cu side), whereas PF_6^- migrated toward the cathode. Alternatively, the discharge process led to ion migration to the opposite direction and left large amounts of dead lithium at the Cu electrode with the formation of an SEI. And based on these findings, this study demonstrated the capability of SIMS to monitor real-time molecular dynamics in liquid electrolytes and visualize SEI and dendrite growth during charge/discharge. In another study, the role of conductive carbon additives on CEI formation and the overall cell performance of a Ni-rich layered oxide cathode ($LiNi_{0.7}Co_{0.15}Mn_{0.15}O_2$) were also investigated by Li et al. [54] by using in situ ToF–SIMS. Here, the region-of-interest sensitive SIMS revealed that a CEI initially forms on the conductive carbon additive with no electrochemical bias applied that can readily passivate cathode particles through the mutual exchange of surface species (Fig. 7d).

3.4.2 Spatially Resolved SEI Chemical Structures by Using Nano-IR

The chemical composition of SEIs is complex and contains numerous organic and inorganic species. And although many compounds have been identified as SEI constituents, information concerning their relative concentration, arrangement, functionality and spatial distribution remains limited.

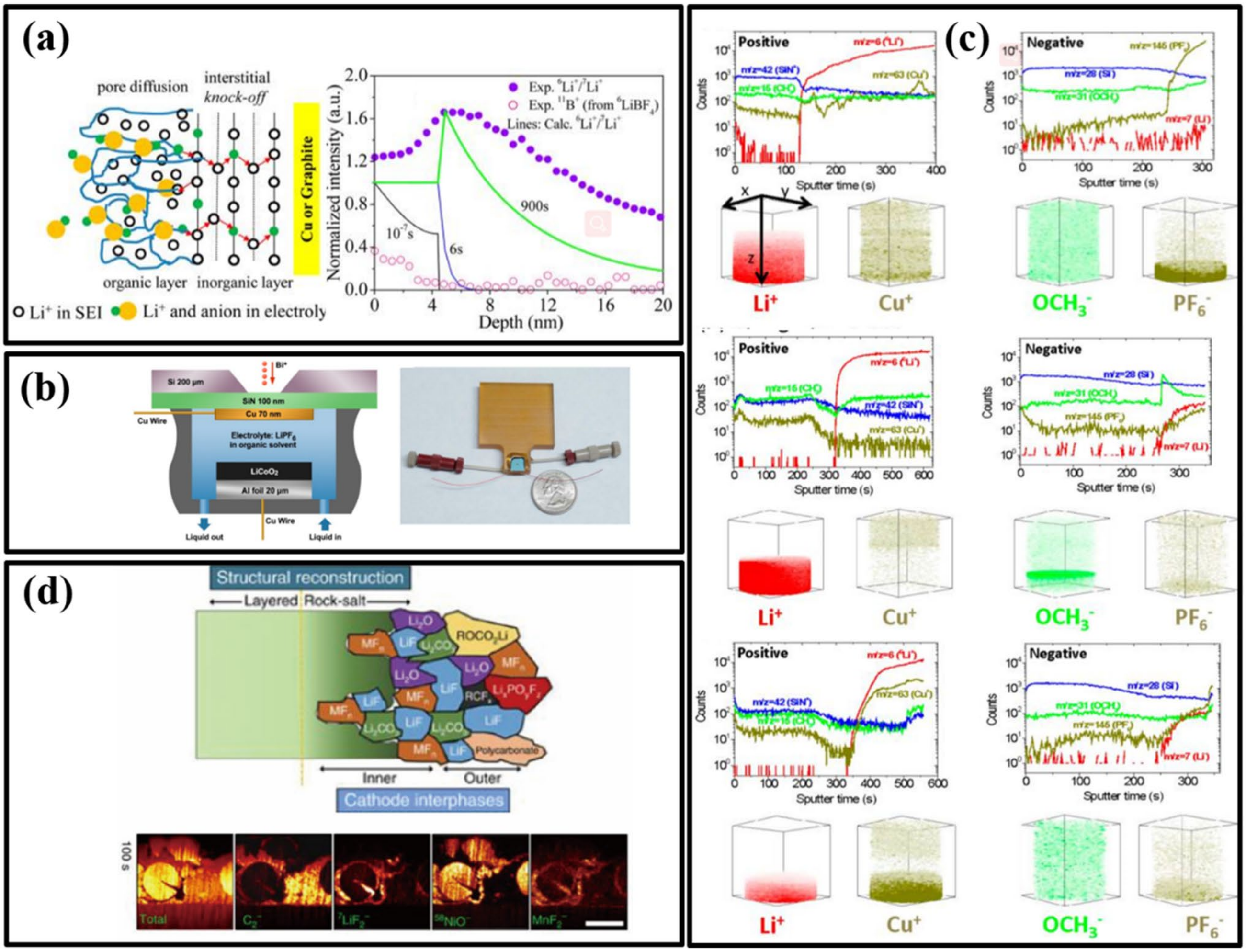

Fig. 7 In situ and ex situ ToF–SIMS for the depth analysis of SEIs. **a** ToF–SIMS depth profiles of $^6Li^+/^7Li^+$ (filled circles) and $^{11}B^+$ (open circles) after soaking the $^7Li^+$ SEI in the $^6LiBF_4$ electrolyte for 900 s (right) and a schematic of the diffusion mechanism of Li^+ through the SEI. The red arrow indicates that only Li^+ can diffuse in the dense inorganic layer through the knockout mechanism (left). Reproduced with permission from Ref. [52] Copyright 2012, American Chemical Society. **b** Schematic of a liquid battery device integrating the anode and the cathode into a liquid battery (left) and a picture of the actual device (right). Copyright 2014, Elsevier. **c** Depth profiles of ToF–SIMS and 3D configurations of several representative positive and negative secondary ions near the anode surface before and after battery charge/discharge. **b**, **c** Reproduced with permission from Ref. [53] Copyright 2015, American Chemical Society. **d** Schematic of the microstructure and chemical composition of surface degradation products at the surface of $LiNi_{0.7}Mn_{0.15}Co_{0.15}O_2$ and cross-sectional views of secondary ions of interest. Reproduced with permission from Ref. [54] Copyright 2017, Springer Nature

Here, vibrational spectroscopy techniques such as FTIR and Raman are useful tools to characterize the molecular bonds of chemical components in SEIs; however, the spatial resolution of FTIR and Raman measurements is usually limited by optical beam sizes, which are in the order of micrometers, whereas SEI compositions are known to be highly heterogeneous at the nanoscale. Therefore, chemical analysis results obtained from FTIR of SEI layers are average values over illuminated areas. To address this, researchers have in recent years developed IR spectroscopic imaging methods with nanometer-scaled spatial resolution (Nano-IR) through three different approaches, including infrared apertureless near-field scanning optical microscopy (IR-aNSOM) [218–220], photothermal induced resonance (PTIR) [221–223] and photoinduced force microscopy (PiFM) [224–226]. And as a result of the unique capabilities of these high-resolution chemical imaging methods, new insights can be gained in the research of SEIs.

In aNSOM, a light beam is focused onto a metallized AFM probe held close to the sample surface [50] to allow light intensity to be strongly enhanced at the probe apex due to local surface plasmonic resonance (Fig. 8a). Here, the scattered signal is modulated by local dielectric properties of the measured sample and is collected from the far field in which different chemical compounds absorb IR differently and thus create image contrast in IR-aNSOM as the AFM tip is scanning over the surface. Based on this, Kostecki et al. [50, 51] pioneered the application of IR-aNSOM in the study of SEIs on Sn and HOPG electrodes. In their first study, an HOPG electrode was cycled in an electrolyte with 1.0 M $LiPF_6$ dissolved in EC/DEC (1:2, in weight ratios) from the OCP (~ 2.9 V) to 0.8 V (before Li ion intercalation into graphite) and samples removed from the electrolyte at 1.66, 1.36 and 0.9 V were chosen for IR-aNSOM measurements at the (002) surface. As a result, these researchers reported that the topography images for the sample discharged to 1.6 V indicated an SEI layer composed of loosely packed 200 nm particles and that the multi-wavelength near-field IR absorption images showed large contrasts, indicating an SEI with a flat inner layer and an outer particle layer and that the two layers possessed distinct but uniform compositions (Fig. 8b). Furthermore, these researchers reported that if discharged to 1.36 V, the morphology of the SEI layer remained similar to that observed at 1.66 V but that the IR images displayed fine granular features at the bottom layer that were not clearly observed in the topography map (Fig. 8c). And if further discharged to 0.9 V, the topography map revealed significantly particle growth and agglomeration in the SEI outer layer, leading to a compact outer film with the inner layer being only observed at a few locations (Fig. 8d).

In their other ex situ IR-aNSOM studies, Kostecki et al. [51] characterized SEI growth on polycrystalline Sn electrodes in which the Sn electrode was scanned several times between OCP (~ 3.0) to 0.8 V versus Li/Li^+ in an electrolyte with 1.0 M $LiPF_6$ in EC/DEC and found that at ~ 1.3 V, the electrolyte was reduced and formed a surface film (Fig. 8e). Here, the researchers found that the SEI was rough and nonuniform and the corresponding IR-aNSOM images showed clear correlation between the specific features and chemical/structural properties of the SEI in which variations in absorbance at different wave numbers strongly indicated an uneven chemical composition on the sample surface on a nanometer length scale (Fig. 8f). These researchers also conducted IR-aNSOM at specific wavelengths corresponding to selected reference compounds to measure specific compound distributions and found a nearly inverted contrast between Li_2CO_3 and lithium ethylene dicarbonate (LEDC) in which Li_2CO_3 was fairly uniformly distributed over the entire SEI except on a few spots and mounds corresponding to the strong signal of LEDC (Fig. 8g).

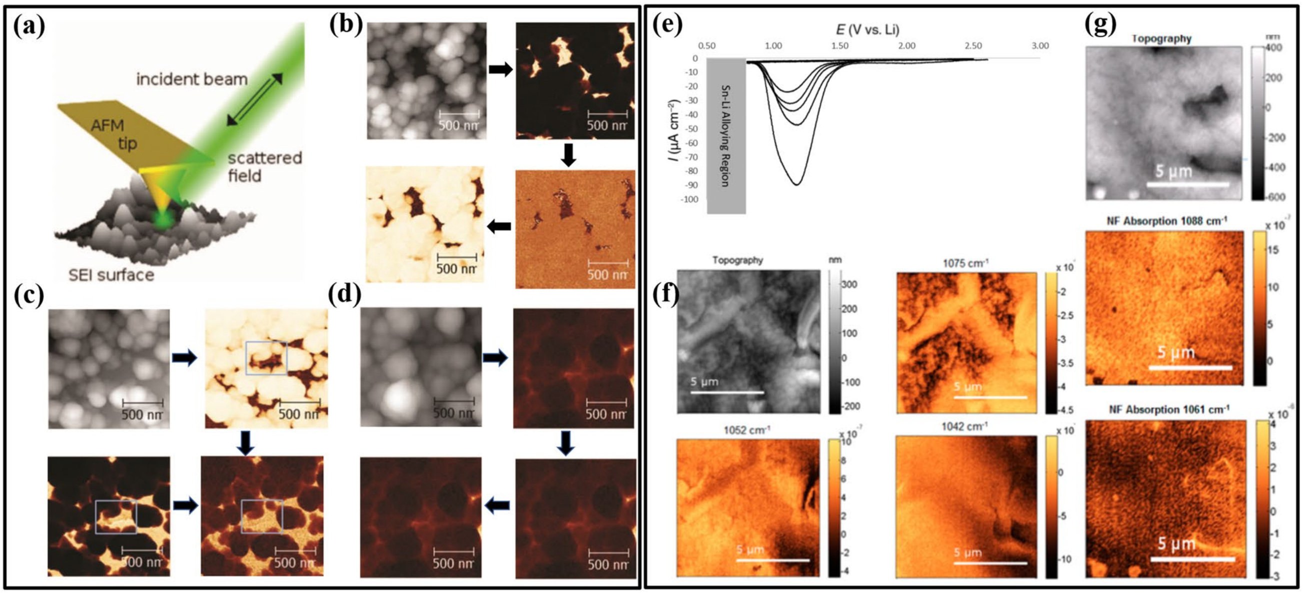

Fig. 8 **a** Schematic of the IR-aNSOM operation. **b** IR-aNSOM images of the SEI layer formed on an HOPG electrode at 1.66 V. In the direction of the arrows are the topological image of the SEI layer and near-field IR absorption images at 1025 cm^{-1}, 1050 cm^{-1} and 1085 cm^{-1}. **c** IR-aNSOM images of the SEI layer formed on the HOPG electrode at 1.36 V. In the direction of the arrows are the topological image of the SEI layer and near-field IR absorption images at 940 cm^{-1}, 1030 cm^{-1} and 1088 cm^{-1}. **d** IR-aNSOM images of the SEI layer formed on the HOPG electrode at 0.9 V. In the direction of the arrows are the topological image of the SEI layer and near-field IR absorption images at 950 cm^{-1}, 1030 cm^{-1} and 1088 cm^{-1}. **a-d** Reproduced with permission from Ref. [50] Copyright 2015, The Electrochemical Society. CV results of a polycrystalline tin electrode in a 1.0 M $LiPF_6$/(EC + DEC) electrolyte (**e**) and their corresponding topological images of the SEI layer and near-field infrared absorption pattern at the same wave number (**f**). **g** Topography of SEI and near-field IR absorption images at 1088 cm^{-1} (carbonate peak) and 1061 cm^{-1} (lithium ethylene dicarbonate peak). **e–g** Reproduced with permission from Ref. [51] Copyright 2015, American Chemical Society

3.4.3 SEI Structures in Their Native State as Determined by Cryo-TEM

Although conventional TEM can obtain atomically resolved images of material structures, it is not ideal for SEI characterization because the SEI layer is chemically reactive and sensitive to electron-beam irradiation. Therefore, much of the current understanding of SEIs obtained from traditional TEM has been limited to the micrometer scale without detailed crystallographic structures. Recently however, several studies have achieved the atomic-resolution imaging of SEIs in their native state using cryogenic electron microscopy (cryo-EM) by freezing the target specimen in liquid nitrogen to preserve the native structure [55–59, 227–231]. For example, Cui et al. [55] characterized the detailed structure of Li metal and its SEI using a cryo-transfer method developed based on cryo-EM procedures used in the field of structural biology in which Li metal was electrochemically deposited onto a copper TEM grid followed by rinsing with the electrolyte and being flash-frozen in liquid nitrogen to preserve the relevant structure and chemical states. As a result, Li dendrite structures were successfully observed with resolution of 0.7 Å (Fig. 9a), demonstrating that the atomically solved imaging of SEIs in their native states was possible.

Concurrently, Meng et al. [56] studied Li metal and corresponding SEIs using cryo-EM inspired by biological imaging techniques and found that the structure of the

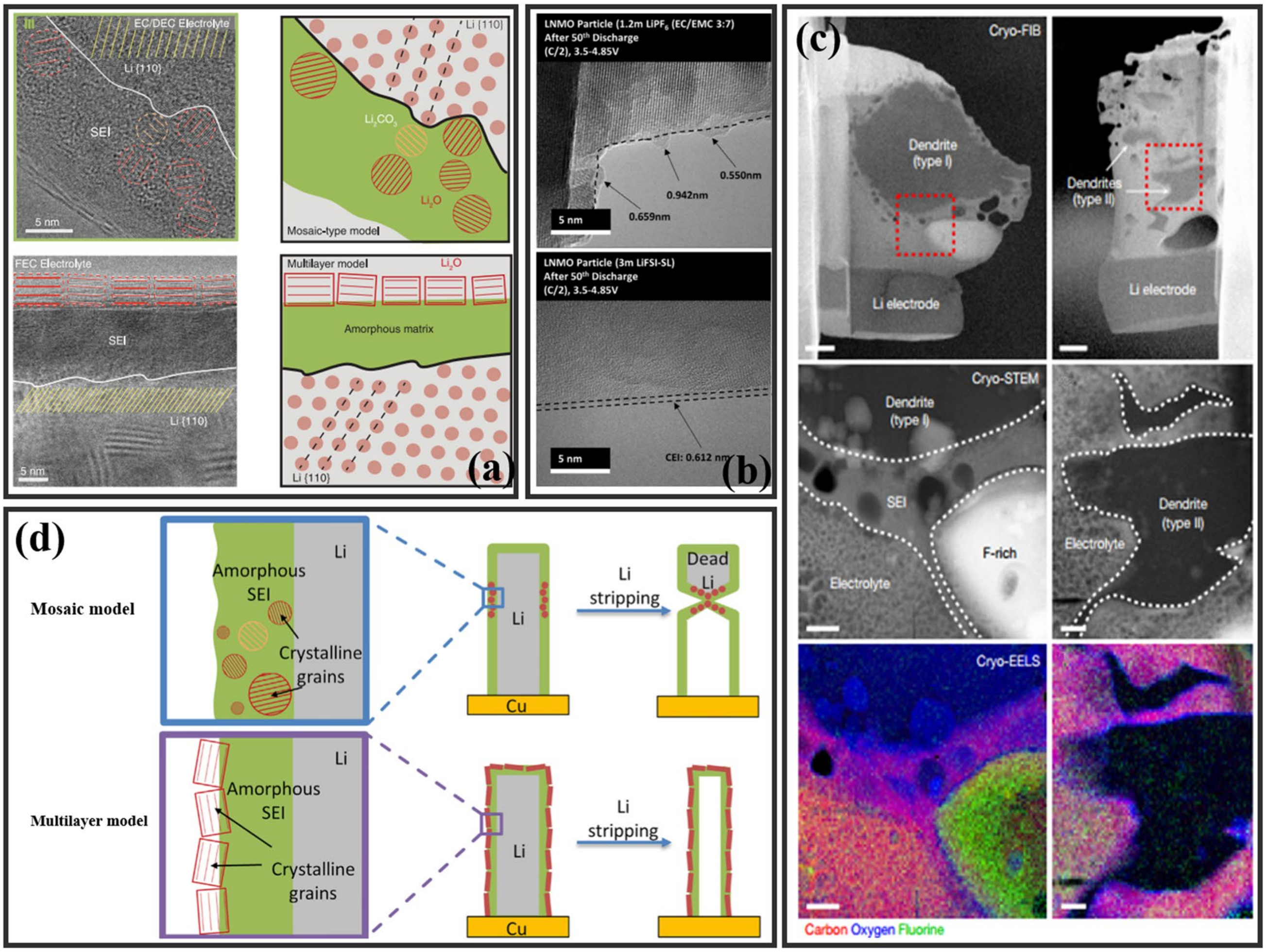

Fig. 9 Cryo-TEM for SEI structures in their native states. **a** Schematics of the mosaic SEI and multilayer SEI nanostructures formed on Li-metal anodes in an EC/DEC electrolyte and a 10 vol% FEC-containing electrolyte. Reproduced with permission from Ref. [55] Copyright 2017, The American Association for the Advancement of Science. **b** Cryo-TEM images of LNMO particle CEIs after discharging for 50 cycles with 1.2 M LiPF$_6$/(EC + EMC, 3:7) (top) and 3 M LiFSI-SL (bottom). Reproduced with permission from Ref. [57] Copyright 2018, Elsevier. **c** Observations of the structure and elemental composition of two different dendrites (type I: left and type II: right) and their interphase layers by using cryo-FIB, cryo-STEM and cryo-EELS. Reproduced with permission from Ref. [58] Copyright 2018, Springer Nature. **d** Atomic-resolution images of the SEI (mosaic structure) formed in the EC-DEC electrolyte (top) and the SEI (multilayer structure) formed in the FEC electrolyte (bottom). Reproduced with permission from Ref. [59] Copyright 2018, Elsevier

electrochemically deposited Li in a 1.0 M $LiPF_6$/EC + EMC electrolyte was amorphous and that the SEI was uneven and consisted of crystalline LiF and amorphous organic species. In addition, these researchers also found that the addition of functional metal ions into the electrolyte can allow for the regulation of SEI properties on Li and improve Coulombic efficiencies during cycling, confirming the importance of the full electrode surface coverage with SEI films as well as the questionable effects of LiF on the SEI performance. Despite this, this study demonstrated that cryo-TEM is a powerful tool in the characterization of fragile, cycled electrodes and can be used to gain fundamental understandings of structural information. As for the exploration of electrolytes for high-voltage LIBs, Xu et al. [57] also used cryo-STEM to preserve the CEI structure/chemistry of a $LiNi_{0.5}Mn_{1.5}O_4$ (LNMO) cathode and avoid beam damage and found that the CEI on the LNMO cathode cycled in the baseline electrolyte exhibited significant variations in thickness and uniformity, whereas the CEI in the studied electrolyte was thin and uniform (Fig. 9b).

Kourkoutis et al. [58] also mapped electrode/electrolyte interfaces and dendrites in Li-metal batteries using cryo-STEM in which cryo-FIB was exploited to prepare cross sections of liquid–solid interfaces for cryo-STEM investigation. As a result, two types of lithium dendrites were found to coexist on lithium anodes, each with distinct structures and chemical compositions (Fig. 9c) in which an extended SEI layer was observed on the first type of dendrites, whereas no SEIs were present on the second type. Here, the researchers found that the extended SEI layer was ~ 300–500 nm thick, which was much thicker than commonly reported thicknesses (tens of nanometers), suggesting that a soft, extended portion of the SEI could be removed through the typical rinsing and drying of samples in preparation protocols. In addition, these researchers found that only the remaining thin, compact layer of the SEI was observed through traditional characterization methods, indicating that more lithium was irreversibly lost to the SEI layer than previously thought. Furthermore, these researchers studied the chemical nature of the Li dendrites and SEIs using cryo-EELS and found that the extended SEI on the type I dendrites possessed increased concentrations of oxygen and lithium as compared with the electrolyte and contained essentially no fluorine. More importantly, the type II dendrites contained lithium hydride rather than Li, which is a major contributor to the loss of battery capacity. And based on these results, these researchers proposed and verified that a full-fluoride-type electrolyte could suppress the formation of LiH dendrites and therefore, increase Coulombic efficiencies and greatly reduce capacity fading.

Cui et al. [59] also studied the structure and composition of SEI films on Li metal formed in EC + DEC electrolytes with 10% FEC using cryo-TEM and found that the SEI formed in the baseline EC + DEC electrolyte presented a mosaic structure that contained randomly distributed inorganic crystalline domains of Li oxide and Li carbonate about 3 nm in diameter throughout an amorphous organic polymer matrix that coated the Li metal, whereas the SEI formed in the electrolyte with 10% FEC possessed a multilayer structure with an amorphous polymer inner layer and an outer layer composed of large grains (~ 15 nm) of Li oxide that was consistent with the multilayer model proposed by Aurbach et al. [64] (Fig. 9d). In addition, these researchers found no significant differences in the chemical composition of the SEIs formed in the two electrolytes, suggesting that the effects of the FEC additive might be in the arrangement of chemical species within the SEI film. Furthermore, uniform Li stripping was observed for the lithium anode with the ordered multilayer SEI, which reduced Li loss during battery cycling by a factor of three, indicating that the uniform distribution of crystalline grains is important to ensure even ionic conductivity and uniform Li stripping, thus providing insights for the rational design of electrolyte additives.

3.4.4 Mechanical Elasticity of SEIs Using AFM Force Curves

Aside from being electronic insulators and ionic conductors, SEI/CEI layers also need to be mechanically flexible and robust enough to accommodate electrode volume variation in charge/discharge cycles, especially for conversion reactions and alloying anode materials with large volume expansion (e.g., silicon, tin, lithium metal). This is because fragile SEIs/CEIs will crack during electrode volume change and trigger new SEI formation, which can lead to low Coulombic efficiencies and rapid capacity fading. And although various tools have been developed for the characterization of the morphology and chemistry of SEI/CEI films, techniques to evaluate mechanical properties are lacking. To address this, AFM-based force spectroscopy, a local strain–stress or "nano-indentation" measurement, has been proposed to be uniquely suitable.

For example, Chen et al. [48] were able to obtain quantitative measurements of Young's modulus of SEIs by using AFM force spectroscopy in which SEI films on MnO anodes in a 1.0 M $LiPF_6$ in EC/PC electrolyte at different discharge/charge states were examined by using ex situ AFM imaging. Here, force spectroscopy curves were recorded on different locations on each sample followed by analysis to extract the Young's modulus and thickness of SEI layers. As a result, these researchers found that both the morphological imaging and mechanical response exhibited remarkable inhomogeneity in the SEI films and that Young's modulus of the SEI varied by over two orders of magnitude at randomized locations on the sample. Furthermore, multiple stages of elastic deformation with different moduli were observed on many force curves and were in agreement with the multilayer or mosaic models in which stiff inorganic domains and soft organic domains were both present in the SEI films. Moreover, single-layered and double-layered structures were also found to coexist on the surface of discharged electrodes and the majority of the SEIs were single-layered (Fig. 10a in the left and middle). And as a result, these researchers concluded based on AFM force spectroscopy that in this electrode/electrolyte combination, formed SEI structures were highly heterogeneous and unstable in the initial cycle.

Force spectroscopy measurements were further applied to study the influence of electrolyte additives (i.e., LiBOB, VC and the mixture of the two) on the mechanical property, structure and stability of SEIs on MnO electrodes in which Zhang et al. [49] found that the structure and property of the SEI films were highly inhomogeneous and changed dynamically under different cycling states and with different additives. Here, these researchers also found that the SEI film formed in the $LiPF_6$/PC + EC baseline electrolyte was soft, electrochemically unstable and decomposed if charged back to 3.0 V, whereas the addition of VC enabled the formation of a thick and soft SEI that would only partially decompose upon charging. In addition, the addition of LiBOB additives was found to be able to significantly improve the electrochemical stability of the SEI film but caused the SEI to become highly rigid, whereas a mixture of the two additives can

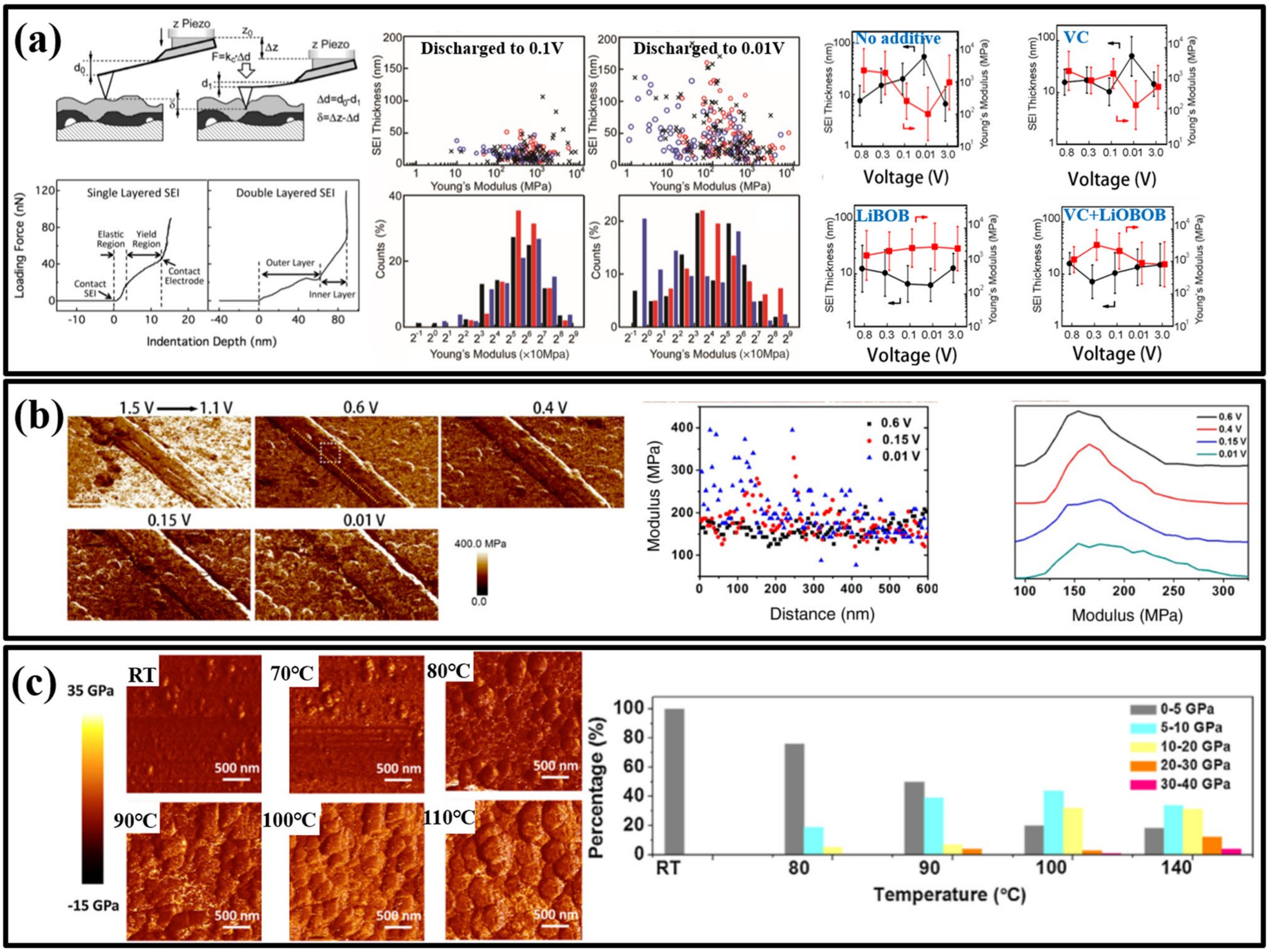

Fig. 10 Mechanical elasticity of SEIs by using AFM. **a** Plots on the left are two typical force curves of single-layered and double-layered SEI films; plots in the middle are the correlations between SEI thickness and Young's modulus for different discharge states. Reproduced with permission from Ref. [48]. Copyright 2012, American Chemical Society. Plots on the right are geometric average values of SEI thickness and Young's modulus on MnO thin-film electrodes in electrolytes without additives, with VC as an additive, with LiBOB as an additive and with VC + LiBOB as an additive. Reproduced with permission from Ref. [49] Copyright 2014, American Chemical Society. **b** From left to right, AFM images of Young's modulus mapping on a single SiNW anode after the first discharge, the distribution of Young's modulus along the dotted yellow line and the statistical value of Young's modulus in the dotted white box. Reproduced with permission from Ref. [47] Copyright 2014, American Chemical Society. **c** AFM images of Young's modulus mapping of the SEI on an HOPG electrode after heating at RT, 70, 80, 90, 100, 110 °C (left) and the distribution of Young's modulus of the SEI after different heating temperatures (right). Reproduced with permission from Ref. [46] Copyright 2018, Elsevier

combine advantages and produce a stable SEI with moderate thickness and stiffness (Fig. 10a). In another study, Li et al. [65] investigated SEI microstructures and mapped Young's modulus of the SEI formed on a silicon anode using the ex situ scanning force curve method and found that SEI thicknesses varied in a range of 0–90 nm during discharge/charge and that the SEI on the silicon anode was highly inhomogeneous with single-, double- and multilayered structures. In addition, these researchers found the existence of porous and sandwiched structures in which soft components tended to grow on the outer layer, which was unstable and decomposed during charging or under increased temperatures. Here, only 51% of the surface of the fully discharged silicon anode was covered by an SEI, whereas full coverage can be obtained through the addition of 2 wt% VC in the electrolyte.

Furthermore, the mechanical properties of SEIs on various electrode materials have also been investigated based on AFM-based force spectroscopy [46, 47, 232–235]. For example, Liu et al. [47] examined the mechanical properties of SEI layers on individual single-crystalline Si nanowire anodes in a 1.0 M $LiPF_6$/PC electrolyte using the peak force quantitative nano-mechanics (PF-QNM) mode of in situ AFM and found that if discharged from 1.5 to 0.6 V, Young's modulus of the SEI changed from 700 to 150 MPa as a result of the thin primary SEI film formation upon discharge (Fig. 10b left). In addition, these researchers found that Young's modulus of the SEI at 0.4 V was similar to that at 0.6 V, but if the potential was swept to 0.15 V, Young's modulus increased slightly and became nonuniform, possibly due to the growth of a thick and particle-like SEI on the nanowire surface. Moreover, these researchers found that the modulus became more inhomogeneous if further discharged to 0.01 V and that the statistical average and dispersion of the modulus increased slightly during the growth of the SEI (Fig. 10b), indicating that the structure and composition of the SEI on SiNW changed dynamically, which was consistent with XPS analysis results.

Huang et al. [46] also systematically studied the change in SEI mechanical properties with temperature on an HOPG electrode in a 1.0 M $LiPF_6$/DMC + EC electrolyte using AFM-based force spectroscopy and found that Young's modulus of the SEI increased with temperature (Fig. 10c left) and attributed this to the decomposition of highly unstable components. These researchers also performed statistical analysis to illustrate the trend of modulus evolution in relation to temperature and revealed that from RT to 140 °C, more force curves exhibited high modulus and less force curves exhibited low modulus (Fig. 10c right), indicating that decomposition or conversion products were stiffer than the original organic components formed at room temperature.

4 Summary and Outlook

In this review, recent progress in the characterization of SEIs in LIBs, including investigations into their electrochemical performance, surface feature and morphology, chemical composition and mechanical elasticity has been summarized. Here, electrochemical performances of SEIs are usually characterized using EIS, CV and LSV, whereas morphology characterizations are mainly conducted by using EM and AFM and chemical compositions are measured by using FTIR, Raman, XPS and SIMS. And overall, the common trend in the development of advanced characterization techniques for SEIs is to enhance instrumental resolution (spatial, energy or force resolution) and integrate measurement techniques into the electrochemical operation of batteries in which irrespective of the probes used, such as the electron beam, IR light, the local proximal probe or the ion beam, characterization results are only relevant and reliable if the samples are scrutinized under conditions as close as possible to their native or operando states.

Because the choices of promising cathode and anode materials for next-generation batteries are limited, the rational control of electrode interfaces may become a critical factor in the development of battery technologies. Therefore, the fundamental understanding of SEI/CEI structures and properties based on advanced characterization techniques is key and further improvements in this area to enhance battery research include the following:

Simultaneous characterization of multiple properties The simultaneous characterization of the morphology and chemical composition of SEIs/CEIs along with the mapping of ionic conductivity and mechanical elasticity is vital to obtain consistent and comprehensive understandings of the SEI/CEI.

Developing in operando characterization methods The development of in operando characterization techniques is vital in the study of SEIs/CEIs. This is because the majority of SEI/CEI films are in situ formed on electrodes during initial charge/discharge cycles and SEI/CEI films experience dynamic change during the cycling of batteries.

Characterization of SEIs/CEIs in full battery settings The characterization of SEIs/CEIs in full battery settings can allow for the elucidation of cross talk between cathodes and anodes, especially the effects of transition metal ion dissolution from the cathode on the formation and stability of SEIs on the anode. And although these issues are often neglected or difficult to address, the understanding of which will have far-reaching impacts on the battery industry.

Overall, great progress has been achieved toward the in-depth understanding of SEIs/CEIs in recent years and further efforts on this topic will provide vital contributions to better battery technologies.

Acknowledgements This work was financially supported by the National Natural Science Foundation of China (Grant nos. 21625304 and 21733012), the "Strategic Priority Research Program" of CAS (Grant no. XDA09010600) and the Ministry of Science and Technology (Grant No. 2016YFA0200703).

References

1. Nishi, Y.: Something About Lithium Ion Batteries. Shokabo Press, Tokyo (1997)
2. Chu, S., Majumdar, A.: Opportunities and challenges for a sustainable energy future. Nature **488**, 294–303 (2012). https://doi.org/10.1038/nature11475
3. Vu, A., Qian, Y., Stein, A.: Porous electrode materials for lithium-ion batteries—how to prepare them and what makes them special. Adv. Energy Mater. **2**, 1056–1085 (2012). https://doi.org/10.1002/aenm.201200320
4. Goodenough, J.B., Park, K.S.: The Li-ion rechargeable battery: a perspective. J. Am. Chem. Soc. **135**, 1167–1176 (2013). https://doi.org/10.1021/ja3091438
5. Dunn, B., Kamath, H., Tarascon, J.M.: Electrical energy storage for the grid: a battery of choices. Science **334**, 928–935 (2011)
6. Dey, A.: Film formation on lithium anode in propylene carbonate. J. Electrochem. Soc. **117**, C248 (1970)
7. Peled, E.: The electrochemical behavior of alkali and alkaline earth metals in nonaqueous battery systems—the solid electrolyte interphase model. J. Electrochem. Soc. **126**, 2047–2051 (1979)
8. Besenhard, J., Winter, M., Yang, J., et al.: Filming mechanism of lithium-carbon anodes in organic and inorganic electrolytes. J. Power Sources **54**, 228–231 (1995)
9. Fong, R., Von Sacken, U., Dahn, J.R.: Studies of lithium intercalation into carbons using nonaqueous electrochemical cells. J. Electrochem. Soc. **137**, 2009–2013 (1990). https://doi.org/10.1149/1.2086855
10. Cheng, X.B., Zhang, R., Zhao, C.Z., et al.: A review of solid electrolyte interphases on lithium metal anode. Adv. Sci. (Weinh) **3**, 1500213 (2016). https://doi.org/10.1002/advs.201500213
11. Choi, N.S., Yew, K.H., Lee, K.Y., et al.: Effect of fluoroethylene carbonate additive on interfacial properties of silicon thin-film electrode. J. Power Sources **161**, 1254–1259 (2006). https://doi.org/10.1016/j.jpowsour.2006.05.049
12. He, Y.B., Liu, M., Huang, Z.D., et al.: Effect of solid electrolyte interface (SEI) film on cyclic performance of $Li_4Ti_5O_{12}$ anodes for Li ion batteries. J. Power Sources **239**, 269–276 (2013). https://doi.org/10.1016/j.jpowsour.2013.03.141
13. Li, N.W., Yin, Y.X., Yang, C.P., et al.: An artificial solid electrolyte interphase layer for stable lithium metal anodes. Adv. Mater. **28**, 1853–1858 (2016). https://doi.org/10.1002/adma.201504526
14. Peled, E., Menachem, C., Bar-Tow, D., et al.: Improved graphite anode for lithium-ion batteries chemically bonded solid electrolyte interface and nanochannel formation. J. Electrochem. Soc. **143**, L4–L7 (1996). https://doi.org/10.1149/1.1836372
15. Sazhin, S.V., Gering, K.L., Harrup, M.K., et al.: Highly quantitative electrochemical characterization of non-aqueous electrolytes and solid electrolyte interphases. J. Electrochem. Soc. **161**, A393–A402 (2014). https://doi.org/10.1149/2.043403jes
16. Broussely, M., Herreyre, S., Biensan, P., et al.: Aging mechanism in Li ion cells and calendar life predictions. J. Power Sources **97**, 13–21 (2001)
17. An, S.J., Li, J., Du, Z., et al.: Fast formation cycling for lithium ion batteries. J. Power Sources **342**, 846–852 (2017). https://doi.org/10.1016/j.jpowsour.2017.01.011
18. Wang, F.M., Wang, H.Y., Yu, M.H., et al.: Differential pulse effects of solid electrolyte interface formation for improving performance on high-power lithium ion battery. J. Power Sources **196**, 10395–10400 (2011). https://doi.org/10.1016/j.jpowsour.2011.08.045
19. Miao, R., Yang, J., Feng, X., et al.: Novel dual-salts electrolyte solution for dendrite-free lithium-metal based rechargeable batteries with high cycle reversibility. J. Power Sources **271**, 291–297 (2014). https://doi.org/10.1016/j.jpowsour.2014.08.011
20. Schmitz, R.W., Murmann, P., Schmitz, R., et al.: Investigations on novel electrolytes, solvents and SEI additives for use in lithium-ion batteries: systematic electrochemical characterization and detailed analysis by spectroscopic methods. Prog. Solid State Ch. **42**, 65–84 (2014). https://doi.org/10.1016/j.progsolidstchem.2014.04.003
21. Xu, C., Lindgren, F., Philippe, B., et al.: Improved performance of the silicon anode for Li-ion batteries: understanding the surface modification mechanism of fluoroethylene carbonate as an effective electrolyte additive. Chem. Mater. **27**, 2591–2599 (2015). https://doi.org/10.1021/acs.chemmater.5b00339
22. Xu, M., Zhou, L., Hao, L., et al.: Investigation and application of lithium difluoro(oxalate)borate (LiDFOB) as additive to improve the thermal stability of electrolyte for lithium-ion batteries. J. Power Sources **196**, 6794–6801 (2011). https://doi.org/10.1016/j.jpowsour.2010.10.050
23. Zhang, X.Q., Cheng, X.B., Chen, X., et al.: Fluoroethylene carbonate additives to render uniform Li deposits in lithium metal batteries. Adv. Funct. Mater. **27**, 1605989 (2017). https://doi.org/10.1002/adfm.201605989
24. Ota, H., Sakata, Y., Inoue, A., et al.: Analysis of vinylene carbonate derived SEI layers on graphite anode. J. Electrochem. Soc. **151**, A1659–A1669 (2004)
25. Nowak, S., Winter, M.: Chemical analysis for a better understanding of aging and degradation mechanisms of non-aqueous electrolytes for lithium ion batteries: method development, application and lessons learned. J. Electrochem. Soc. **162**, A2500–A2508 (2015)
26. Xu, G., Liu, Z., Zhang, C., et al.: Strategies for improving the cyclability and thermo-stability of $LiMn_2O_4$-based batteries at elevated temperatures. J. Mater. Chem. A **3**, 4092–4123 (2015)
27. Wang, L., Chen, B., Ma, J., et al.: Reviving lithium cobalt oxide-based lithium secondary batteries-toward a higher energy density. Chem. Soc. Rev. **47**, 6505–6602 (2018)
28. Haregewoin, A.M., Wotango, A.S., Hwang, B.J.: Electrolyte additives for lithium ion battery electrodes: progress and perspectives. Energy Environ. Sci. **9**, 1955–1988 (2016). https://doi.org/10.1039/c6ee00123h
29. Heins, T.P., Harms, N., Schramm, L.S., et al.: Development of a new electrochemical impedance spectroscopy approach for monitoring the solid electrolyte interphase formation. Energy Technol. **4**, 1509–1513 (2016)
30. Yoon, S., Kim, H., Cho, J.J., et al.: Lactam derivatives as solid electrolyte interphase forming additives for a graphite anode of lithium-ion batteries. J. Power Sources **244**, 711–715 (2013). https://doi.org/10.1016/j.jpowsour.2012.11.115
31. Liu, T., Lin, L., Bi, X., et al.: In situ quantification of interphasial chemistry in Li-ion battery. Nat. Nanotechnol. **14**, 50–56 (2018). https://doi.org/10.1038/s41565-018-0284-y
32. Zhang, S.S., Xu, K., Jow, T.R.: EIS study on the formation of solid electrolyte interface in Li-ion battery. Electrochim. Acta **51**, 1636–1640 (2006). https://doi.org/10.1016/j.electacta.2005.02.137
33. Aurbach, D., Gamolsky, K., Markovsky, B., et al.: On the use of vinylene carbonate (VC) as an additive to electrolyte solutions for Li-ion batteries. Electrochim. Acta **47**, 1423–1439 (2002)

34. Lee, S.H., You, H.G., Han, K.S., et al.: A new approach to surface properties of solid electrolyte interphase on a graphite negative electrode. J. Power Sources **247**, 307–313 (2014). https://doi.org/10.1016/j.jpowsour.2013.08.105
35. Strelcov, E., Cothren, J., Leonard, D., et al.: In situ SEM study of lithium intercalation in individual V_2O_5 nanowires. Nanoscale **7**, 3022–3027 (2015). https://doi.org/10.1039/c4nr06767c
36. Bordes, A., Eom, K., Fuller, T.F.: The effect of fluoroethylene carbonate additive content on the formation of the solid-electrolyte interphase and capacity fade of Li-ion full-cell employing nano Si–graphene composite anodes. J. Power Sources **257**, 163–169 (2014). https://doi.org/10.1016/j.jpowsour.2013.12.144
37. Liao, B., Li, H., Xu, M., et al.: Designing low impedance interface films simultaneously on anode and cathode for high energy batteries. Adv. Energy Mater. **8**, 1800802 (2018). https://doi.org/10.1002/aenm.201800802
38. Liu, X.H., Wang, J.W., Huang, S., et al.: In situ atomic-scale imaging of electrochemical lithiation in silicon. Nat. Nanotechnol. **7**, 749–756 (2012). https://doi.org/10.1038/nnano.2012.170
39. Mehdi, B.L., Qian, J., Nasybulin, E., et al.: Observation and quantification of nanoscale processes in lithium batteries by operando electrochemical (S)TEM. Nano Lett. **15**, 2168–2173 (2015). https://doi.org/10.1021/acs.nanolett.5b00175
40. Lucas, I.T., Pollak, E., Kostecki, R.: In situ AFM studies of SEI formation at a Sn electrode. Electrochem. Commun. **11**, 2157–2160 (2009). https://doi.org/10.1016/j.elecom.2009.09.019
41. Chan, C.K., Ruffo, R., Hong, S.S., et al.: Surface chemistry and morphology of the solid electrolyte interphase on silicon nanowire lithium-ion battery anodes. J. Power Sources **189**, 1132–1140 (2009). https://doi.org/10.1016/j.jpowsour.2009.01.007
42. Malmgren, S., Ciosek, K., Hahlin, M., et al.: Comparing anode and cathode electrode/electrolyte interface composition and morphology using soft and hard X-ray photoelectron spectroscopy. Electrochim. Acta **97**, 23–32 (2013). https://doi.org/10.1016/j.electacta.2013.03.010
43. Nandasiri, M.I., Camacho-Forero, L.E., Schwarz, A.M., et al.: In situ chemical imaging of solid-electrolyte interphase layer evolution in Li–S batteries. Chem. Mater. **29**, 4728–4737 (2017). https://doi.org/10.1021/acs.chemmater.7b00374
44. Park, Y., Shin, S.H., Hwang, H., et al.: Investigation of solid electrolyte interface (SEI) film on $LiCoO_2$ cathode in fluoroethylene carbonate (FEC)-containing electrolyte by 2D correlation X-ray photoelectron spectroscopy (XPS). J. Mol. Struct. **1069**, 157–163 (2014). https://doi.org/10.1016/j.molstruc.2014.01.041
45. Shi, F., Ross, P.N., Zhao, H., et al.: A catalytic path for electrolyte reduction in lithium-ion cells revealed by in situ attenuated total reflection-Fourier transform infrared spectroscopy. J. Am. Chem. Soc. **137**, 3181–3184 (2015). https://doi.org/10.1021/ja5128456
46. Huang, S., Cheong, L.Z., Wang, D., et al.: Thermal stability of solid electrolyte interphase of lithium-ion batteries. Appl. Surf. Sci. **454**, 61–67 (2018). https://doi.org/10.1016/j.apsusc.2018.05.136
47. Liu, X.R., Deng, X., Liu, R.R., et al.: Single nanowire electrode electrochemistry of silicon anode by in situ atomic force microscopy: solid electrolyte interphase growth and mechanical properties. ACS Appl. Mater. Inter. **6**, 20317–20323 (2014). https://doi.org/10.1021/am505847s
48. Zhang, J., Wang, R., Yang, X., et al.: Direct observation of inhomogeneous solid electrolyte interphase on MnO anode with atomic force microscopy and spectroscopy. Nano Lett. **12**, 2153–2157 (2012). https://doi.org/10.1021/nl300570d
49. Zhang, J., Yang, X., Wang, R., et al.: Influences of additives on the formation of a solid electrolyte interphase on MnO electrode studied by atomic force microscopy and force spectroscopy. J. Phys. Chem. C **118**, 20756–20762 (2014). https://doi.org/10.1021/jp503953n
50. Ayache, M., Jang, D., Syzdek, J., et al.: Near-field IR nanoscale imaging of the solid electrolyte interphase on a HOPG electrode. J. Electrochem. Soc. **162**, A7078–A7082 (2015). https://doi.org/10.1149/2.0101513jes
51. Ayache, M., Lux, S.F., Kostecki, R.: IR near-field study of the solid electrolyte interphase on a tin electrode. J. Phys. Chem. Lett. **6**, 1126–1129 (2015). https://doi.org/10.1021/acs.jpclett.5b00263
52. Shi, S., Lu, P., Liu, Z., et al.: Direct calculation of Li-ion transport in the solid electrolyte interphase. J. Am. Chem. Soc. **134**, 15476–15487 (2012). https://doi.org/10.1021/ja305366r
53. Zhu, Z., Zhou, Y., Yan, P., et al.: In situ mass spectrometric determination of molecular structural evolution at the solid electrolyte interphase in lithium-ion batteries. Nano Lett. **15**, 6170–6176 (2015). https://doi.org/10.1021/acs.nanolett.5b02479
54. Yuan, Y., Amine, K., Lu, J., et al.: Understanding materials challenges for rechargeable ion batteries with in situ transmission electron microscopy. Nat. Commun. **8**, 15806 (2017). https://doi.org/10.1038/ncomms15806
55. Li, Y., Li, Y., Pei, A., et al.: Atomic structure of sensitive battery materials and interfaces revealed by cryo-electron microscopy. Science **358**, 506–510 (2017)
56. Wang, X., Zhang, M., Alvarado, J., et al.: New insights on the structure of electrochemically deposited lithium metal and its solid electrolyte interphases via cryogenic TEM. Nano Lett. **17**, 7606–7612 (2017)
57. Alvarado, J., Schroeder, M.A., Zhang, M., et al.: A carbonate-free, sulfone-based electrolyte for high-voltage Li-ion batteries. Mater. Today **21**, 341–353 (2018). https://doi.org/10.1016/j.mattod.2018.02.005
58. Zachman, M.J., Tu, Z., Choudhury, S., et al.: Cryo-STEM mapping of solid-liquid interfaces and dendrites in lithium-metal batteries. Nature **560**, 345–349 (2018). https://doi.org/10.1038/s41586-018-0397-3
59. Li, Y., Huang, W., Li, Y., et al.: Correlating structure and function of battery interphases at atomic resolution using cryoelectron microscopy. Joule **2**, 2167–2177 (2018). https://doi.org/10.1016/j.joule.2018.08.004
60. Goodenough, J.B., Kim, Y.: Challenges for rechargeable Li batteries. Chem. Mater. **22**, 587–603 (2009)
61. Delp, S.A., Borodin, O., Olguin, M., et al.: Importance of reduction and oxidation stability of high voltage electrolytes and additives. Electrochim. Acta **209**, 498–510 (2016). https://doi.org/10.1016/j.electacta.2016.05.100
62. Peled, E., Golodnitsky, D., Ardel, G.: Advanced model for solid electrolyte interphase electrodes in liquid and polymer electrolytes. J. Electrochem. Soc. **144**, L208–L210 (1997)
63. Ein-Eli, Y.: A new perspective on the formation and structure of the solid electrolyte interface at the graphite anode of Li-ion cells. Electrochem. Solid-State Lett. **2**, 212–214 (1999)
64. Zaban, A., Aurbach, D.: Impedance spectroscopy of lithium and nickel electrodes in propylene carbonate solutions of different lithium salts a comparative study. J. Power Sources **54**, 289–295 (1995)
65. Zheng, J., Zheng, H., Wang, R., et al.: 3D visualization of inhomogeneous multi-layered structure and Young's modulus of the solid electrolyte interphase (SEI) on silicon anodes for lithium ion batteries. Phys. Chem. Chem. Phys. **16**, 13229–13238 (2014). https://doi.org/10.1039/c4cp01968g
66. Winter, M.: The solid electrolyte interphase–the most important and the least understood solid electrolyte in rechargeable Li batteries. Z. Phys. Chem. **223**, 1395–1406 (2009)
67. An, S.J., Li, J., Daniel, C., et al.: The state of understanding of the lithium-ion-battery graphite solid electrolyte interphase (SEI) and its relationship to formation cycling. Carbon **105**, 52–76 (2016)

68. Kim, S.P., Van Duin, A.C., Shenoy, V.B.: Effect of electrolytes on the structure and evolution of the solid electrolyte interphase (SEI) in Li-ion batteries: a molecular dynamics study. J. Power Sources **196**, 8590–8597 (2011)
69. Lu, P., Harris, S.J.: Lithium transport within the solid electrolyte interphase. Electrochem. Commun. **13**, 1035–1037 (2011). https://doi.org/10.1016/j.elecom.2011.06.026
70. Guan, P., Liu, L., Lin, X.: Simulation and experiment on solid electrolyte interphase (SEI) morphology evolution and lithium-ion diffusion. J. Electrochem. Soc. **162**, A1798–A1808 (2015)
71. Shi, S., Qi, Y., Li, H., et al.: Defect thermodynamics and diffusion mechanisms in Li_2CO_3 and implications for the solid electrolyte interphase in Li-ion batteries. J. Phys. Chem. C **117**, 8579–8593 (2013)
72. Gu, Y., Wang, W.W., Li, Y.J., et al.: Designable ultra-smooth ultra-thin solid-electrolyte interphases of three alkali metal anodes. Nature Commun. **9**, 1339 (2018)
73. Gauthier, M., Carney, T.J., Grimaud, A., et al.: Electrode-electrolyte interface in Li-ion batteries: current understanding and new insights. J. Phys. Chem. Lett. **6**, 4653–4672 (2015). https://doi.org/10.1021/acs.jpclett.5b01727
74. Aurbach, D., Zinigrad, E., Cohen, Y., et al.: A short review of failure mechanisms of lithium metal and lithiated graphite anodes in liquid electrolyte solutions. Solid State Ionics **148**, 405–416 (2002)
75. Aurbach, D.: Review of selected electrode–solution interactions which determine the performance of Li and Li ion batteries. J. Power Sources **89**, 206–218 (2000)
76. Aurbach, D., Markovsky, B., Levi, M., et al.: New insights into the interactions between electrode materials and electrolyte solutions for advanced nonaqueous batteries. J. Power Sources **81**, 95–111 (1999)
77. Collins, J., Gourdin, G., Foster, M., et al.: Carbon surface functionalities and SEI formation during Li intercalation. Carbon **92**, 193–244 (2015). https://doi.org/10.1016/j.carbon.2015.04.007
78. Nie, M., Lucht, B.L.: Role of lithium salt on solid electrolyte interface (SEI) formation and structure in lithium ion batteries. J. Electrochem. Soc. **161**, A1001–A1006 (2014)
79. Peled, E., Golodnitsky, D., Ulus, A., et al.: Effect of carbon substrate on SEI composition and morphology. Electrochim. Acta **50**, 391–395 (2004)
80. Ensling, D., Stjerndahl, M., Nytén, A., et al.: A comparative XPS surface study of Li_2FeSiO_4/C cycled with LiTFSI-and LiPF 6-based electrolytes. J. Mater. Chem. **19**, 82–88 (2009)
81. Balbuena, P.B., Wang, Y.: Lithium-Ion Batteries: Solid-Electrolyte Interphase. Imperial College Press, London (2004)
82. Wang, C., Kakwan, I., Appleby, A.J., et al.: In situ investigation of electrochemical lithium intercalation into graphite powder. J. Electroanal. Chem. **489**, 55–67 (2000)
83. Philippe, B., Dedryvère, R.M., Gorgoi, M., et al.: Role of the $LiPF_6$ salt for the long-term stability of silicon electrodes in Li-ion batteries—a photoelectron spectroscopy study. Chem. Mater. **25**, 394–404 (2013)
84. Cherkashinin, G., Motzko, M., Schulz, N., et al.: Electron spectroscopy study of Li[Ni Co, Mn]O_2/electrolyte interface: electronic structure, interface composition, and device implications. Chem. Mater. **27**, 2875–2887 (2015). https://doi.org/10.1021/cm5047534
85. Jarry, A., Gottis, S., Yu, Y.S., et al.: The formation mechanism of fluorescent metal complexes at the $Li_xNi_{0.5}Mn_{1.5}O_{(4-\delta)}$/carbonate ester electrolyte interface. J. Am. Chem. Soc. **137**, 3533–3539 (2015). https://doi.org/10.1021/ja5116698
86. Domi, Y., Ochida, M., Tsubouchi, S., et al.: In situ AFM study of surface film formation on the edge plane of HOPG for lithium-ion batteries. J. Phys. Chem. C **115**, 25484–25489 (2011). https://doi.org/10.1021/jp2064672
87. Dedryvère, R., Leroy, S., Martinez, H., et al.: XPS valence characterization of lithium salts as a tool to study electrode/electrolyte interfaces of Li-ion batteries. J. Phys. Chem. B **110**, 12986–12992 (2006)
88. Nie, M., Chalasani, D., Abraham, D.P., et al.: Lithium ion battery graphite solid electrolyte interphase revealed by microscopy and spectroscopy. J. Phys. Chem. C **117**, 1257–1267 (2013)
89. Zhuang, G.V., Yang, H., Ross, P.N., et al.: Lithium methyl carbonate as a reaction product of metallic lithium and dimethyl carbonate. Electrochem. Solid-State Lett. **9**, A64–A68 (2006)
90. Zhao, L., Watanabe, I., Doi, T., et al.: TG-MS analysis of solid electrolyte interphase (SEI) on graphite negative-electrode in lithium-ion batteries. J. Power Sources **161**, 1275–1280 (2006). https://doi.org/10.1016/j.jpowsour.2006.05.045
91. Xu, K., Zhuang, G.V., Allen, J.L., et al.: Syntheses and characterization of lithium alkyl mono-and dicarbonates as components of surface films in Li-ion batteries. J. Phys. Chem. B **110**, 7708–7719 (2006)
92. Ein-Eli, Y., Markovsky, B., Aurbach, D., et al.: The dependence of the performance of Li-C intercalation anodes for Li-ion secondary batteries on the electrolyte solution composition. Electrochim. Acta **39**, 2559–2569 (1994)
93. Aurbach, D., Levi, M.D., Levi, E., et al.: Failure and stabilization mechanisms of graphite electrodes. J. Phys. Chem. B **101**, 2195–2206 (1997)
94. Zhuang, G.V., Xu, K., Yang, H., et al.: Lithium ethylene dicarbonate identified as the primary product of chemical and electrochemical reduction of EC in 1.2 M $LiPF_6$/EC: EMC electrolyte. J. Phys. Chem. B **109**, 17567–17573 (2005)
95. Aurbach, D., Markovsky, B., Shechter, A., et al.: A comparative study of synthetic graphite and Li electrodes in electrolyte solutions based on ethylene carbonate–dimethyl carbonate mixtures. J. Electrochem. Soc. **143**, 3809–3820 (1996)
96. Besenhard, J., Wagner, M., Winter, M., et al.: Inorganic film-forming electrolyte additives improving the cycling behaviour of metallic lithium electrodes and the self-discharge of carbon—lithium electrodes. J. Power Sources **44**, 413–420 (1993)
97. Komaba, S., Kaplan, B., Ohtsuka, T., et al.: Inorganic electrolyte additives to suppress the degradation of graphite anodes by dissolved Mn(II) for lithium-ion batteries. J. Power Sources **119**, 378–382 (2003)
98. Shin, J.S., Han, C.H., Jung, U.H., et al.: Effect of Li_2CO_3 additive on gas generation in lithium-ion batteries. J. Power Sources **109**, 47–52 (2002)
99. Möller, K.C., Santner, H., Kern, W., et al.: In situ characterization of the SEI formation on graphite in the presence of a vinylene group containing film-forming electrolyte additives. J. Power Sources **119**, 561–566 (2003)
100. Leggesse, E.G., Jiang, J.C.: Theoretical study of the reductive decomposition of 1, 3-propane sultone: SEI forming additive in lithium-ion batteries. RSC Adv. **2**, 5439–5446 (2012)
101. Aurbach, D., Ein-Eli, Y., Markovsky, B., et al.: The study of electrolyte solutions based on ethylene and diethyl carbonates for rechargeable Li batteries II. Graphite electrodes. J. Electrochem. Soc. **142**, 2882–2890 (1995)
102. Zhang, S.S.: A review on electrolyte additives for lithium-ion batteries. J. Power Sources **162**, 1379–1394 (2006). https://doi.org/10.1016/j.jpowsour.2006.07.074
103. Dahbi, M., Violleau, D., Ghamouss, F., et al.: Interfacial properties of LiTFSI and $LiPF_6$-based electrolytes in binary and ternary mixtures of alkylcarbonates on graphite electrodes and celgard separator. Ind. Eng. Chem. Res. **51**, 5240–5245 (2012). https://doi.org/10.1021/ie203066x
104. Han, H.B., Zhou, S.S., Zhang, D.J., et al.: Lithium bis(fluorosulfonyl)imide (LiFSI) as conducting salt for nonaqueous liquid electrolytes for lithium-ion batteries:

physicochemical and electrochemical properties. J. Power Sources **196**, 3623–3632 (2011)

105. Plakhotnyk, A.V., Ernst, L., Schmutzler, R.: Hydrolysis in the system $LiPF_6$–propylene carbonate–dimethyl carbonate–H_2O. J. Fluorine Chem. **126**, 27–31 (2005)
106. Kawamura, T., Kimura, A., Egashira, M., et al.: Thermal stability of alkyl carbonate mixed-solvent electrolytes for lithium ion cells. J. Power Sources **104**, 260–264 (2002)
107. Fu, L.J., Liu, H., Li, C., et al.: Surface modifications of electrode materials for lithium ion batteries. Solid State Sci. **8**, 113–128 (2006). https://doi.org/10.1016/j.solidstatesciences.2005.10.019
108. Petibon, R., Sinha, N., Burns, J., et al.: Comparative study of electrolyte additives using electrochemical impedance spectroscopy on symmetric cells. J. Power Sources **251**, 187–194 (2014)
109. Chan, C.K., Peng, H., Liu, G., et al.: High-performance lithium battery anodes using silicon nanowires. Nat. Nanotechnol. **3**, 31–35 (2008). https://doi.org/10.1038/nnano.2007.411
110. Wu, H., Cui, Y.: Designing nanostructured Si anodes for high energy lithium ion batteries. Nano Today **7**, 414–429 (2012). https://doi.org/10.1016/j.nantod.2012.08.004
111. Winter, M., Novák, P., Monnier, A.: Graphites for lithium-ion cells: the correlation of the first-cycle charge loss with the Brunauer–Emmett–Teller surface area. J. Electrochem. Soc. **145**, 428–436 (1998)
112. Zheng, T., Gozdz, A.S., Amatucci, G.G.: Reactivity of the solid electrolyte interface on carbon electrodes at elevated temperatures. J. Electrochem. Soc. **146**, 4014–4018 (1999)
113. Ng, S.H., Vix-Guterl, C., Bernardo, P., et al.: Correlations between surface properties of graphite and the first cycle specific charge loss in lithium-ion batteries. Carbon **47**, 705–712 (2009). https://doi.org/10.1016/j.carbon.2008.11.008
114. Novák, P., Ufheil, J., Buqa, H., et al.: The importance of the active surface area of graphite materials in the first lithium intercalation. J. Power Sources **174**, 1082–1085 (2007). https://doi.org/10.1016/j.jpowsour.2007.06.036
115. Spahr, M.E., Buqa, H., Würsig, A., et al.: Surface reactivity of graphite materials and their surface passivation during the first electrochemical lithium insertion. J. Power Sources **153**, 300–311 (2006). https://doi.org/10.1016/j.jpowsour.2005.05.032
116. Eshkenazi, V., Peled, E., Burstein, L., et al.: XPS analysis of the SEI formed on carbonaceous materials. Solid State Ionics **170**, 83–91 (2004). https://doi.org/10.1016/s0167-2738(03)00107-3
117. Tsubouchi, S., Domi, Y., Doi, T., et al.: Spectroscopic characterization of surface films formed on edge plane graphite in ethylene carbonate-based electrolytes containing film-forming additives. J. Electrochem. Soc. **159**, A1786–A1790 (2012)
118. Peled, E., Golodnitsky, D., Menachem, C., et al.: An advanced tool for the selection of electrolyte components for rechargeable lithium batteries. J. Electrochem. Soc. **145**, 3482–3486 (1998)
119. Li, J., Murphy, E., Winnick, J., et al.: The effects of pulse charging on cycling characteristics of commercial lithium-ion batteries. J. Power Sources **102**, 302–309 (2001)
120. Ogihara, N., Igarashi, Y., Kamakura, A., et al.: Disordered carbon negative electrode for electrochemical capacitors and high-rate batteries. Electrochim. Acta **52**, 1713–1720 (2006). https://doi.org/10.1016/j.electacta.2006.01.082
121. Zhang, S.S.: The effect of the charging protocol on the cycle life of a Li-ion battery. J. Power Sources **161**, 1385–1391 (2006). https://doi.org/10.1016/j.jpowsour.2006.06.040
122. Wang, Y., Zaghib, K., Guerfi, A., et al.: Accelerating rate calorimetry studies of the reactions between ionic liquids and charged lithium ion battery electrode materials. Electrochim. Acta **52**, 6346–6352 (2007)
123. Lu, W., Lee, C., Venkatachalapathy, R., et al.: Electrochemical and thermal behaviour of $LiNi_{0.8}Co_{0.2}O_2$ cathode in sealed 18650 Li-ion cells. J. Appl. Electrochem. **30**, 1119–1124 (2000)
124. Aurbach, D., Daroux, M., Faguy, P., et al.: Identification of surface films formed on lithium in propylene carbonate solutions. J. Electrochem. Soc. **134**, 1611–1620 (1987)
125. Aurbach, D., Gofer, Y., Ben-Zion, M., et al.: The behaviour of lithium electrodes in propylene and ethylene carbonate: Te major factors that influence Li cycling efficiency. J. Electroanal. Chem. **339**, 451–471 (1992)
126. Zhang, L., Zhang, K., Shi, Z., et al.: LiF as an artificial SEI layer to enhance the high-temperature cycle performance of $Li_4Ti_5O_{12}$. Langmuir **33**, 11164–11169 (2017). https://doi.org/10.1021/acs.langmuir.7b02031
127. Steinhauer, M., Risse, S., Wagner, N., et al.: Investigation of the solid electrolyte interphase formation at graphite anodes in lithium-ion batteries with electrochemical impedance spectroscopy. Electrochim. Acta **228**, 652–658 (2017). https://doi.org/10.1016/j.electacta.2017.01.128
128. Zhang, J.N., Li, Q., Wang, Y., et al.: Dynamic evolution of cathode electrolyte interphase (CEI) on high voltage $LiCoO_2$ cathode and its interaction with Li anode. Energy Storage Mater. **14**, 1–7 (2018). https://doi.org/10.1016/j.ensm.2018.02.016
129. Sun, D., Wang, Q., Zhou, J. et al. : Forming a Stable CEI Layer on LiNi0. 5Mn1. 5O4 Cathode by theSynergy Effect of FEC and HDI. J. Electrochem. Soc. **165**, A2032–A2036 (2018)
130. Zhao, W., Zheng, J., Zou, L., et al.: High voltage operation of Ni-rich NMC cathodes enabled by stable electrode/electrolyte interphases. Adv. Energy Mater. **8**, 1800297 (2018)
131. He, Y.B., Li, B., Yang, Q.H. et al. : Effects of current densities on the formation of LiCoO2/graphitelithium ion battery. J. Solid State Electr. **15**, 1977–1985 (2010)
132. Zheng, M.S., Dong, Q.F., Cai, H.Q., et al.: Formation and influence factors of solid electrolyte interphase film on the negative electrode surface in lithium-ion batteries. J. Electrochem. Soc. **152**, A2207–A2210 (2005)
133. Zhang, X., Kostecki, R., Richardson, T.J., et al.: Electrochemical and infrared studies of the reduction of organic carbonates. J. Electrochem. Soc. **148**, A1341–A1345 (2001)
134. Schroder, K.W., Celio, H., Webb, L.J. et al.: Examining solid electrolyte interphase formation oncrystalline silicon electrodes: influence of electrochemical preparation and ambient exposureconditions. J. Phys. Chem. C **116**, 19737–19747 (2012)
135. Lindgren, F., Xu, C., Niedzicki, L., et al.: SEI formation and interfacial stability of a Si electrode in a LiTDI-salt based electrolyte with FEC and VC additives for Li-ion batteries. ACS Appl. Mater. Inter. **8**, 15758–15766 (2016). https://doi.org/10.1021/acsami.6b02650
136. Tsuda, T., Kanetsuku, T., Sano, T., et al.: In situ SEM observation of the Si negative electrode reaction in an ionic-liquid-based lithium-ion secondary battery. Microscopy **64**, 159–168 (2015). https://doi.org/10.1093/jmicro/dfv003
137. Waldmann, T., Wilka, M., Kasper, M., et al.: Temperature dependent ageing mechanisms in Lithium-ion batteries—a post-mortem study. J. Power Sources **262**, 129–135 (2014). https://doi.org/10.1016/j.jpowsour.2014.03.112
138. Zhuang, Q., Tian, L., Wei, G., et al.: Two-and three-electrode impedance spectroscopic studies of graphite electrode in the first lithiation. Sci. Bull. **54**, 2627–2632 (2009). https://doi.org/10.1007/s11434-009-0356-3
139. Chen, L., Wang, K., Xie, X., et al.: Effect of vinylene carbonate (VC) as electrolyte additive on electrochemical performance of Si film anode for lithium ion batteries. J. Power Sources **174**, 538–543 (2007). https://doi.org/10.1016/j.jpowsour.2007.06.149

140. Kominato, A., Yasukawa, E., Sato, N., et al.: Analysis of surface films on lithium in various organic electrolytes. J. Power Sources **68**, 471–475 (1997)
141. Huang, Z., Ren, J., Zhang, W., et al.: Protecting the Li–metal anode in a Li–O_2 battery by using boric acid as an SEI-forming additive. Adv. Mater. **30**, 1803270 (2018)
142. Goktas, M., Bolli, C., Berg, E.J., et al.: Graphite as cointercalation electrode for sodium-ion batteries: electrode dynamics and the missing solid electrolyte interphase (SEI). Adv. Energy Mater. **8**, 1702724 (2018)
143. Zhang, H.L., Liu, C., Tan, J., et al.: New insight into the solid electrolyte interphase with use of a focused ion beam. J. Phys. Chem. B **109**, 22205–22211 (2005)
144. Joshi, T., Eom, K., Yushin, G., et al.: Effects of dissolved transition metals on the electrochemical performance and SEI growth in lithium-ion batteries. J. Electrochem. Soc. **161**, A1915–A1921 (2014)
145. Etiemble, A., Tranchot, A., Douillard, T., et al.: Evolution of the 3D microstructure of a Si-Based electrode for Li-Ion batteries investigated by FIB/SEM tomography. J. Electrochem. Soc. **163**, A1550–A1559 (2016)
146. Xiao, X., Liu, Z., Baggetto, L., et al.: Unraveling manganese dissolution/deposition mechanisms on the negative electrode in lithium ion batteries. Phys. Chem. Chem. Phys. **16**, 10398–10402 (2014)
147. Wang, C.M., Xu, W., Liu, J., et al.: In situ transmission electron microscopy and spectroscopy studies of interfaces in Li ion batteries: challenges and opportunities. J. Mater. Res. **25**, 1541–1547 (2010)
148. Sui, T., Song, B., Dluhos, J., et al.: Nanoscale chemical mapping of Li-ion battery cathode material by FIB-SEM and TOF-SIMS multi-modal microscopy. Nano Energy **17**, 254–260 (2015). https://doi.org/10.1016/j.nanoen.2015.08.013
149. Sun, Y., Zheng, G., Seh, Z.W., et al.: Graphite-encapsulated Li-metal hybrid anodes for high-capacity Li batteries. Chem **1**, 287–297 (2016)
150. Unocic, R.R., Sun, X.G., Sacci, R.L., et al.: Direct visualization of solid electrolyte interphase formation in lithium-ion batteries with in situ electrochemical transmission electron microscopy. Microsc. Microanal. **20**, 1029–1037 (2014). https://doi.org/10.1017/S1431927614012744
151. Zeng, Z., Zhang, X., Bustillo, K., et al.: In Situ Study of Lithiation and Delithiation of MoS_2 Nanosheets Using Electrochemical Liquid Cell Transmission Electron Microscopy. Nano Lett. **15**, 5214–5220 (2015). https://doi.org/10.1021/acs.nanolett.5b02483
152. Cheong, J.Y., Chang, J.H., Seo, H.K., et al.: Growth dynamics of solid electrolyte interphase layer on SnO_2 nanotubes realized by graphene liquid cell electron microscopy. Nano Energy **25**, 154–160 (2016)
153. Gu, M., Parent, L.R., Mehdi, B.L., et al.: Demonstration of an electrochemical liquid cell for operando transmission electron microscopy observation of the lithiation/delithiation behavior of Si nanowire battery anodes. Nano Lett. **13**, 6106–6112 (2013). https://doi.org/10.1021/nl403402q
154. Li, Z., Tan, X., Li, P., et al.: Coupling in situ TEM and ex situ analysis to understand heterogeneous sodiation of antimony. Nano Lett. **15**, 6339–6348 (2015)
155. Nie, M., Abraham, D.P., Chen, Y., et al.: Silicon solid electrolyte interphase (SEI) of lithium ion battery characterized by microscopy and spectroscopy. J. Phys. Chem. C **117**, 13403–13412 (2013). https://doi.org/10.1021/jp404155y
156. Chattopadhyay, S., Lipson, A.L., Karmel, H.J., et al.: In situ X-ray study of the solid electrolyte interphase (SEI) formation on graphene as a model Li-ion battery anode. Chem. Mater. **24**, 3038–3043 (2012). https://doi.org/10.1021/cm301584r
157. Sacci, R.L., Dudney, N.J., More, K.L., et al.: Direct visualization of initial SEI morphology and growth kinetics during lithium deposition by in situ electrochemical transmission electron microscopy. Chem. Commun. **50**, 2104–2107 (2014). https://doi.org/10.1039/c3cc49029g
158. Yang, T., Zhang, N., Lang, Y., et al.: Enhanced rate performance of carbon-coated $LiNi_{0.5}Mn_{1.5}O_4$ cathode material for lithium ion batteries. Electrochim. Acta **56**, 4058–4064 (2011). https://doi.org/10.1016/j.electacta.2010.12.109
159. Zeng, Z., Liang, W.I., Liao, H.G., et al.: Visualization of electrode-electrolyte interfaces in $LiPF_6$/EC/DEC electrolyte for lithium ion batteries via in situ TEM. Nano Lett. **14**, 1745–1750 (2014). https://doi.org/10.1021/nl403922u
160. Leenheer, A.J., Jungjohann, K.L., Zavadil, K.R., et al.: Lithium electrodeposition dynamics in aprotic electrolyte observed in situ via transmission electron microscopy. ACS Nano **9**, 4379–4389 (2015)
161. Dolle, M., Grugeon, S., Beaudoin, B., et al.: In situ TEM study of the interface carbon/electrolyte. J. Power Sources **97**, 104–106 (2001)
162. Yuk, J.M., Seo, H.K., Choi, J.W., et al.: Anisotropic lithiation onset in silicon nanoparticle anode revealed by in situ graphene liquid cell electron microscopy. ACS Nano **8**, 7478–7485 (2014)
163. Jungjohann, K., Harrison, K., Goriparti, S., et al.: In-situ S/TEM of Li-ion batteries: lithium metal and sn anode interfacial processes. Microsc. Microanal. **24**, 1484–1485 (2018). https://doi.org/10.1017/s1431927618007900
164. Sacci, R.L., Black, J.M., Balke, N., et al.: Nanoscale imaging of fundamental Li battery chemistry: solid-electrolyte interphase formation and preferential growth of lithium metal nanoclusters. Nano Lett. **15**, 2011–2018 (2015). https://doi.org/10.1021/nl5048626
165. Wang, F., Graetz, J., Moreno, M.S., et al.: Chemical distribution and bonding of lithium in intercalated graphite: identification with optimized electron energy loss spectroscopy. ACS Nano **5**, 1190–1197 (2011)
166. Deng, X., Liu, X., Yan, H., et al.: Morphology and modulus evolution of graphite anode in lithium ion battery: an in situ AFM investigation. Sci. China Chem. **57**, 178–183 (2013). https://doi.org/10.1007/s11426-013-4988-4
167. Jeong, S.K., Inaba, M., Iriyama, Y., et al.: Surface film formation on a graphite negative electrode in lithium-ion batteries: AFM study on the effects of co-solvents in ethylene carbonate-based solutions. Electrochim. Acta **47**, 1975–1982 (2002)
168. Alliata, D., Kötz, R., Novák, P., et al.: Electrochemical SPM investigation of the solid electrolyte interphase film formed on HOPG electrodes. Electrochem. Commun. **2**, 436–440 (2000)
169. Novák, P., Joho, F., Lanz, M., et al.: The complex electrochemistry of graphite electrodes in lithium-ion batteries. J. Power Sources **97**, 39–46 (2001)
170. Edström, K., Herranen, M.: Thermal stability of the HOPG/liquid electrolyte interphase studied by in situ electrochemical atomic force microscopy. J. Electrochem. Soc. **147**, 3628–3632 (2000)
171. Koltypin, M., Cohen, Y.S., Markovsky, B., et al.: The study of lithium insertion–deinsertion processes into composite graphite electrodes by in situ atomic force microscopy (AFM). Electrochem. Commun. **4**, 17–23 (2002)
172. Liu, X.R., Wang, L., Wan, L.J., et al.: In situ observation of electrolyte-concentration-dependent solid electrolyte interphase on graphite in dimethyl sulfoxide. ACS Appl. Mater. Interfaces. **7**, 9573–9580 (2015). https://doi.org/10.1021/acsami.5b01024
173. Mogi, R., Inaba, M., Jeong, S.K., et al.: Effects of some organic additives on lithium deposition in propylene carbonate. J. Electrochem. Soc. **149**, A1578–A1583 (2002)

174. Morigaki, K.I.: In situ analysis of the interfacial reactions between MCMB electrode and organic electrolyte solutions. J. Power Sources **103**, 253–264 (2002)
175. Huang, S., Wang, S., Hu, G., et al.: Modulation of solid electrolyte interphase of lithium-ion batteries by LiDFOB and LiBOB electrolyte additives. Appl. Surf. Sci. **441**, 265–271 (2018). https://doi.org/10.1016/j.apsusc.2018.02.014
176. Lin, L., Yang, K., Tan, R., et al.: Effect of sulfur-containing additives on the formation of a solid-electrolyte interphase evaluated by in situ AFM and ex situ characterizations. J. Mater. Chem. A **5**, 19364–19370 (2017). https://doi.org/10.1039/c7ta05469f
177. Haruta, M., Kijima, Y., Hioki, R., et al.: Artificial lithium fluoride surface coating on silicon negative electrodes for the inhibition of electrolyte decomposition in lithium-ion batteries: visualization of a solid electrolyte interphase using in situ AFM. Nanoscale **10**, 17257–17264 (2018)
178. Wang, M., Huai, L., Hu, G., et al.: Effect of LiFSI concentrations to form thickness-and modulus-controlled SEI layers on lithium metal anodes. J. Phys. Chem. C **122**, 9825–9834 (2018)
179. Domi, Y., Ochida, M., Tsubouchi, S., et al.: Electrochemical AFM observation of the HOPG edge plane in ethylene carbonate-based electrolytes containing film-forming additives. J. Electrochem. Soc. **159**, A1292–A1297 (2012)
180. Tokranov, A., Sheldon, B.W., Li, C., et al.: In situ atomic force microscopy study of initial solid electrolyte interphase formation on silicon electrodes for Li-ion batteries. ACS Appl. Mater. Inter. **6**, 6672–6686 (2014). https://doi.org/10.1021/am500363t
181. Li, L., Xu, J., Han, S., et al.: Study on the intrinsic properties of the interface between the cathode and the electrolyte of high voltage LNMO. J. Electrochem. **22**, 582–589 (2016)
182. Doi, T., Inaba, M., Tsuchiya, H., et al.: Electrochemical AFM study of $LiMn_2O_4$ thin film electrodes exposed to elevated temperatures. J. Power Sources **180**, 539–545 (2008). https://doi.org/10.1016/j.jpowsour.2008.02.054
183. Kitta, M., Kohyama, M.: Stability of the $LiMn_2O_4$ surface in a $LiPF_6$-based non-aqueous electrolyte studied by in situ atomic force microscopy. Jpn. J. Appl. Phys. **55**, 065801 (2016). https://doi.org/10.7567/jjap.55.065801
184. Lu, W., Zhang, J., Xu, J., et al.: In situ visualized cathode electrolyte interphase on $LiCoO_2$ in high voltage cycling. ACS Appl. Mater. Inter. **9**, 19313–19318 (2017)
185. Liu, R.R., Deng, X., Liu, X.R., et al.: Facet dependent SEI formation on the $LiNi_{0.5}Mn_{1.5}O_4$ cathode identified by in situ single particle atomic force microscopy. Chem. Commun. **50**, 15756–15759 (2014)
186. Quinlan, F.T., Sano, K., Willey, T., et al.: Surface characterization of the spinel $Li_xMn_2O_4$ cathode before and after storage at elevated temperatures. Chem. Mater. **13**, 4207–4212 (2001)
187. Clemencon, A., Appapillai, A., Kumar, S., et al.: Atomic force microscopy studies of surface and dimensional changes in Li_xCoO_2 crystals during lithium de-intercalation. Electrochim. Acta **52**, 4572–4580 (2007)
188. Verde, M.G., Baggetto, L., Balke, N., et al.: Elucidating the phase transformation of $Li_4Ti_5O_{12}$ lithiation at the nanoscale. ACS Nano **10**, 4312–4321 (2016)
189. Luo, W., Lin, C.F., Zhao, O., et al.: Ultrathin surface coating enables the stable sodium metal anode. Adv. Energy Mater. **7**, 1601526 (2017). https://doi.org/10.1002/aenm.201601526
190. LaCourse, W.R., Dasenbrock, C.O.: Column liquid chromatography: equipment and instrumentation. Anal. Chem. **70**, 37–52 (1998)
191. Aurbach, D.: The electrochemical behavior of lithium salt solutions of γ-butyrolactone with noble metal electrodes. J. Electrochem. Soc. **136**, 906–913 (1989)
192. Aurbach, D.: Electrode–solution interactions in Li-ion batteries: a short summary and new insights. J. Power Sources **119–121**, 497–503 (2003). https://doi.org/10.1016/s0378-7753(03)00273-8
193. Cheng, H., Zhu, C., Lu, M., et al.: In situ micro-FTIR study of the solid–solid interface between lithium electrode and polymer electrolytes. J. Power Sources **174**, 1027–1031 (2007)
194. Parry, D.B., Samant, M.G., Seki, H., et al.: In situ Fourier transform infrared spectroelectrochemical study of bisulfate and sulfate adsorption on gold, with and without the underpotential deposition of copper. Langmuir **9**, 1878–1887 (1993)
195. Korepp, C., Santner, H., Fujii, T., et al.: 2-Cyanofuran—a novel vinylene electrolyte additive for PC-based electrolytes in lithium-ion batteries. J. Power Sources **158**, 578–582 (2006)
196. Santner, H., Korepp, C., Winter, M., et al.: In-situ FTIR investigations on the reduction of vinylene electrolyte additives suitable for use in lithium-ion batteries. Anal. Bioanal. Chem. **379**, 266–271 (2004)
197. Morigaki, K.I., Ohta, A.: Analysis of the surface of lithium in organic electrolyte by atomic force microscopy, Fourier transform infrared spectroscopy and scanning auger electron microscopy. J. Power Sources **76**, 159–166 (1998)
198. Pyun, S.I., Ryu, Y.G.: In-situ spectroelectrochemical analysis of the passivating surface film formed on a graphite electrode during the electrochemical reduction of lithium salts and organic carbonate solvent. J. Electroanal. Chem. **455**, 11–17 (1998)
199. Winter, M., Imhof, R., Joho, F., et al.: FTIR and DEMS investigations on the electroreduction of chloroethylene carbonate-based electrolyte solutions for lithium-ion cells. J. Power Sources **81**, 818–823 (1999)
200. Lanz, P., Novák, P.: Combined in situ Raman and IR microscopy at the interface of a single graphite particle with ethylene carbonate/dimethyl carbonate. J. Electrochem. Soc. **161**, A1555–A1563 (2014)
201. Hongyou, K., Hattori, T., Nagai, Y., et al.: Dynamic in situ fourier transform infrared measurements of chemical bonds of electrolyte solvents during the initial charging process in a Li ion battery. J. Power Sources **243**, 72–77 (2013). https://doi.org/10.1016/j.jpowsour.2013.05.192
202. Reiter, J., Vondrák, J., Michálek, J., et al.: Ternary polymer electrolytes with 1-methylimidazole based ionic liquids and aprotic solvents. Electrochim. Acta **52**, 1398–1408 (2006). https://doi.org/10.1016/j.electacta.2006.07.043
203. Yang, J., Solomatin, N., Kraytsberg, A., et al.: In-situ spectroelectrochemical insight revealing distinctive silicon anode solid electrolyte interphase formation in a lithium-ion battery. ChemistrySelect **1**, 572–576 (2016)
204. Matsui, M., Dokko, K., Kanamura, K.: Dynamic behavior of surface film on $LiCoO_2$ thin film electrode. J. Power Sources **177**, 184–193 (2008). https://doi.org/10.1016/j.jpowsour.2007.10.078
205. Matsui, M., Dokko, K., Kanamura, K.: Surface layer formation and stripping process on $LiMn_2O_4$ and $LiNi_{1/2}Mn_{3/2}O_4$ thin film electrodes. J. Electrochem. Soc. **157**, A121–A129 (2010)
206. Matsui, M., Dokko, K., Akita, Y., et al.: Surface layer formation of $LiCoO_2$ thin film electrodes in non-aqueous electrolyte containing lithium bis (oxalate) borate. J. Power Sources **210**, 60–66 (2012)
207. Matsushita, T., Dokko, K., Kanamura, K.: In situ FT-IR measurement for electrochemical oxidation of electrolyte with ethylene carbonate and diethyl carbonate on cathode active material used in rechargeable lithium batteries. J. Power Sources **146**, 360–364 (2005). https://doi.org/10.1016/j.jpowsour.2005.03.011
208. Ratner, B.D., Castner, D.G.: Electron Spectroscopy for Chemical Analysis. Surface Analysis: the Principal Techniques. Wiley, Hoboken (2009)
209. Song, H., Zheng, C., Zhang, Z., et al.: Effect of vinylene carbonate as electrolyte additive on cycling performance of

LiFePO$_4$/graphite cell at elevated temperature. T. Nonferr. Metal. Soc. **24**, 723–728 (2014)

210. Maibach, J., Xu, C., Eriksson, S.K., et al.: A high pressure X-ray photoelectron spectroscopy experimental method for characterization of solid-liquid interfaces demonstrated with a Li-ion battery system. Rev. Sci. Instrum. **86**, 044101 (2015)
211. Tang, C.Y., Haasch, R.T., Dillon, S.J.: In situ X-ray photoelectron and Auger electron spectroscopic characterization of reaction mechanisms during Li-ion cycling. Chem. Commun. **52**, 13257–13260 (2016). https://doi.org/10.1039/c6cc08176b
212. Wenzel, S., Randau, S., Leichtweiß, T., et al.: Direct observation of the interfacial instability of the fast ionic conductor Li$_{10}$GeP$_2$S$_{12}$ at the lithium metal anode. Chem. Mater. **28**, 2400–2407 (2016)
213. Benninghoven, A.: Die analyse monomolekularer Festkörperoberflächenschichten mit Hilfe der Sekundärionenemission. Zeitschrift für Physik A Hadrons and Nuclei **230**, 403–417 (1970)
214. McPhail, D.: Applications of secondary ion mass spectrometry (SIMS) in materials science. J. Mater. Sci. **41**, 873–903 (2006)
215. Van Vaeck, L., Adriaens, A., Gijbels, R.: Static secondary ion mass spectrometry (S-SIMS) Part 1: methodology and structural interpretation. Mass Spectrom. Rev. **18**, 1–47 (1999)
216. Peled, E., Tow, D.B., Merson, A., et al.: Microphase structure of SEI on HOPG. J. New Mater. Electrochem. Syst. **3**, 319–326 (2000)
217. Pereira-Nabais, C., Światowska, J., Chagnes, A., et al.: Interphase chemistry of Si electrodes used as anodes in Li-ion batteries. Appl. Surf. Sci. **266**, 5–16 (2013). https://doi.org/10.1016/j.apsusc.2012.10.165
218. Zenhausern, F., O'boyle, M., Wickramasinghe, H.: Apertureless near-field optical microscope. Appl. Phys. Lett. **65**, 1623–1625 (1994)
219. Muller, E.A., Pollard, B., Raschke, M.B.: Infrared chemical nano-imaging: accessing structure, coupling, and dynamics on molecular length scales. J. Phys. Chem. Lett. **6**, 1275–1284 (2015)
220. Centrone, A.: Infrared imaging and spectroscopy beyond the diffraction limit. Annu. Rev. Anal. Chem. **8**, 101–126 (2015)
221. Lahiri, B., Holland, G., Centrone, A.: Chemical imaging beyond the diffraction limit: experimental validation of the PTIR technique. Small **9**, 439–445 (2013)
222. Dazzi, A., Prazeres, R., Glotin, F., et al.: Local infrared microspectroscopy with subwavelength spatial resolution with an atomic force microscope tip used as a photothermal sensor. Opt. Lett. **30**, 2388–2390 (2005)
223. Dazzi, A., Prater, C.B.: AFM-IR: technology and applications in nanoscale infrared spectroscopy and chemical imaging. Chem. Rev. **117**, 5146–5173 (2016)
224. Liu, J., Park, S., Nowak, D., et al.: Near-Field characterization of graphene plasmons by photo-induced force microscopy. Laser Photonics Rev. **12**, 1800040 (2018)
225. Almajhadi, M., Wickramasinghe, H.K.: Contrast and imaging performance in photo induced force microscopy. Opt. Express **25**, 26923–26938 (2017)
226. Jahng, J., Ladani, F.T., Khan, R.M., et al.: Complex Light and Optical Forces X. 97641 J. International Society for Optics and Photonics, Bellingham (2016)
227. Wang, X., Li, Y., Meng, Y.S.: Cryogenic electron microscopy for characterizing and diagnosing batteries. Joule **2**, 2225–2234 (2018)
228. Chen, Y., Zheng, L., Johnson, D.C., et al.: Reaction: potential impact of cryo-EM technique on battery industry. Chem **4**, 2254–2256 (2018). https://doi.org/10.1016/j.chempr.2018.09.019
229. Wang, Y.: Cryo-electron microscopy finds place in materials science. Sci. China Mater. **61**, 129–130 (2017). https://doi.org/10.1007/s40843-017-9159-1
230. Yuan, Y., Lu, J.: Reaction: freezing electrochemical interfaces for robustness in electron microscopy. Chem **4**, 2253–2254 (2018). https://doi.org/10.1016/j.chempr.2018.09.010
231. Li, Y., Li, Y., Cui, Y.: Catalyst: how cryo-EM shapes the development of next-generation batteries. Chem **4**, 2250–2252 (2018). https://doi.org/10.1016/j.chempr.2018.09.007
232. Weadock, N., Varongchayakul, N., Wan, J., et al.: Determination of mechanical properties of the SEI in sodium ion batteries via colloidal probe microscopy. Nano Energy **2**, 713–719 (2013). https://doi.org/10.1016/j.nanoen.2013.08.005
233. McAllister, Q.P., Strawhecker, K.E., Becker, C.R., et al.: In situ atomic force microscopy nanoindentation of lithiated silicon nanopillars for lithium ion batteries. J. Power Sources **257**, 380–387 (2014)
234. Lacey, S.D., Wan, J., Cresce, A.V.W., et al.: Atomic force microscopy studies on molybdenum disulfide flakes as sodium-ion anodes. Nano Lett. **15**, 1018–1024 (2015)
235. Liu, X., Wang, D., Wan, L.: Progress of electrode/electrolyte interfacial investigation of Li-ion batteries via in situ scanning probe microscopy. Sci. Bull. **60**, 839–849 (2015). https://doi.org/10.1007/s11434-015-0763-6

Yanli Chu received her Bachelor's degree in 2014 from Henan Normal University. She is now working on her master's degree study in the School of Nano Technology and Nano Bionics, University of Science and Technology of China. Her research focuses on characterizing of solid electrolyte interphases in secondary batteries.

Yanbin Shen received her B.S. from HIT in 2006, and after working as an R&D engineer in Shenzhen BAK battery Co. Ltd. for 4 years, she moved to Aarhus University and got her Ph.D. in 2014. Then, she worked as a postdoctoral research fellow at Syncat@Beijing for two years and joined SINANO as an associate professor in 2017. Her research interests include materials development and mechanism characterization in energy storage systems.

Feng Guo received his Bachelor's and M.Sc. degrees in the College of Materials Science and Engineering, Huaqiao University, in 2012 and 2016, respectively. He is currently a third-year Ph.D. student at SINANO. His current research interests focus on energy storage materials, especially Li-metal anodes.

Xuan Zhao received his B.S. from Yangzhou University in 2015 and M.S. from Yangzhou University in 2018. He joined SINANO as a research assistant in 2018. His research interest is developing electrolyte additives for high-voltage lithium-ion batteries.

Qingyu Dong received his B.S. from Qufu Normal University in 2012. He is currently a master student at Suzhou Institute of Nanotechnology and Nano-Bionics, Chinese Academy of Sciences. His research interests are mainly focusing on electrolyte additives for lithium-ion batteries.

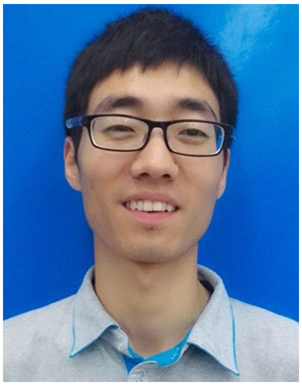

Qingyong Zhang received his B.S. and M.S. degrees from HIT in 2014 and 2016. He is now working as an R&D engineer in Shenzhen BAK battery Co., Ltd. He is interested in energy storage system analysis and simulation.

Wei Li is currently working at Shenzhen BAK battery Co. Ltd. as a senior engineer. He received his M.S. from Harbin Institute of Technology in 2013. His research interests focus on lithium-ion batteries failure and electrochemical mechanism analysis, in particular, electrochemical characterization of materials, electrodes and different prototype cells.

Hui Chen received his M.S. from Harbin Institute of Technology in 2006. He joined Shenzhen BAK Battery Co. Ltd. as an R&D engineer since 2006, and he is now in charge of the R&D department. His research interests focus on lithium-ion batteries development.

Dr. Zhaojun Luo received her Ph.D. from Kunming University in 1999. Then, she worked as a postdoctoral researcher in Central South University for 2 years. From 2001 to 2006, she worked as the director of the Key Laboratory of Composite Materials in Shenzhen. From 2006 to 2011, she mainly engaged in the research of lithium-ion batteries in Shenzhen BAK Battery Co. Ltd. Then, she served as the head of the Energy Storage System Development of Huawei Technologies Co., Ltd. for two years. She is now the assistant chairman and chief technology officer of Shenzhen BAK Battery Co. Ltd. Her research interests include inorganic nonmetallic materials and lithium-ion battery material.

Liwei Chen received his B.S. from USTC in 1993, M.S. from Peking University in 1996 and Ph.D. from Harvard University in 2001. After working as a joint postdoctoral research fellow at Columbia University and IBMT. J. Watson Research Center, he joined the Department of Chemistry and Biochemistry at Ohio University in 2004 as an assistant professor. He moved to SINANO as a professor in 2009. Starting in 2018, he is also affiliated with the School of Chemistry and Chemical Engineering, Shanghai Jiao Tong University, as a Professor of Physical Chemistry. His research interests include materials development and mechanism characterization in energy chemistry.